

A comprehensive framework for assessing the accuracy and uncertainty of global above-ground biomass maps

Arnan Araza^{a,b,*}, Sytze de Bruin^a, Martin Herold^{a,c}, Shaun Quegan^d, Nicolas Labriere^e, Pedro Rodríguez-Veiga^{f,g}, Valerio Avitabile^h, Maurizio Santoroⁱ, Edward T.A. Mitchard^j, Casey M. Ryan^j, Oliver Phillips^k, Simon Willcock^{l,m}, Hans Verbeeckⁿ, Joao Carreiras^d, Lars Hein^b, Mart-Jan Schelhaas^o, Ana Maria Pacheco-Pascagaza^f, Polyanna da Conceição Bispo^p, Gaia Vaglio Laurin^q, Ghislain Vieilledent^r, Ferry Slik^s, Arief Wijaya^t, Simon L. Lewis^{u,v}, Alexandra Morel^w, Jingjing Liang^x, Hansrajie Sukhdeo^y, Dmitry Schepaschenko^{z,aa,ab}, Jura Cavlovic^{ac}, Hammad Gilani^{ad}, Richard Lucas^{ae}

^aLaboratory of Geo-information and Remote sensing, Wageningen University and Research, Droevendaalsesteeg 3, 6708 PB Wageningen, Netherlands

^bEnvironmental Systems Analysis, Wageningen University and Research, Droevendaalsesteeg 3a, 6708 PB Wageningen, Netherlands

^cHelmholtz GFZ German Research Centre for Geosciences, Section 1.4 Remote Sensing and Geoinformatics, Telegrafenberg, Potsdam, 14473, Germany

^dNational Centre for Earth Observation (NCEO) and University of Sheffield, Hicks Building, Sheffield S3 7RH, UK

^eLaboratoire Evolution et Diversité Biologique (EDB), Toulouse cedex 9, France

^fCentre for Landscape and Climate Research, School of Geography, Geology and the Environment, University of Leicester LE1 7RH, UK

^gNCEO and University of Leicester, University Road, Leicester LE1 7RH, UK

^hEuropean Commission, Joint Research Centre (JRC), European Commission, Ispra, Italy

ⁱGamma Remote Sensing, Worbstrasse 225, Gümliigen, Switzerland

^jSchool of GeoSciences, University of Edinburgh, Crew Building, The King's Buildings, EH9 3FF, UK.

^kSchool of Geography, University of Leeds, Woodhouse Lane, Leeds LS2 9JT, UK

^lSchool of Natural Sciences, Bangor University, UK

^mRothamsted Research, West Common, Harpenden AL5 2JQ, UK

ⁿComputational and Applied Vegetation Ecology, Faculty of Bioscience Engineering, Ghent University, Ghent, Belgium

^oWageningen Environmental Research, Wageningen University and Research, Droevendaalsesteeg 3-3 A, 6708 PB Wageningen, Netherlands

^pDepartment of Geography, School of Environment, Education and Development, University of Manchester, Manchester, UK

^qDepartment for Innovation in Biological, Agro-food, and Forestry Systems, Tuscia University, Viterbo, Italy

^rAMAP, Univ Montpellier, CIRAD, CNRS, INRAE, IRD, Montpellier, France

^sEnvironmental and Life Sciences, Faculty of Science, Universiti Brunei Darussalam, Brunei Darussalam

^tForest and the Ocean, World Resources Institute Indonesia, Jakarta, Indonesia

^uDept Geography, University College London School of Geography, London WC1E 6BT, UK

^vUniversity of Leeds, Woodhouse, Leeds LS2 9JT, UK

^wSchool of Geography and Environmental Sciences, University of Dundee, Nethergate, Dundee, DD1 4HN

^xDepartment of Forestry and Natural Resources, Purdue University, USA

^yGuyana Forestry Commission, 1 Water Street Kingston, Georgetown, Guyana

^zInternational Institute for Applied Systems Analysis, Austria

^{aa}Center of Forest Ecology and Productivity of the Russian Academy of Sciences, Russia

^{ab}Institute of Ecology and Geography, Siberian Federal University, Russia

^{ac}University of Zagreb, Faculty of Forestry, Department of Forest Inventory and Management, Croatia

^{ad}Institute of Space Technology, 1 Islamabad Highway, Islamabad, 44000, Pakistan

^{ae}Department of Geography and Earth Sciences, Aberystwyth University, Aberystwyth, Ceredigion SY23 3DB, UK

*Correspondence

Email address: arnan.araza@wur.nl (Arnan Araza)

Abstract

Over the past decade, several global maps of above-ground biomass (AGB) have been produced, but they exhibit significant differences that reduce their value for climate and carbon cycle modelling, and also for national estimates of forest carbon stocks and their changes. The number of such maps is anticipated to increase because of new satellite missions dedicated to measuring AGB. Objective and consistent methods to estimate the accuracy and uncertainty of AGB maps are therefore urgently needed. This paper develops and demonstrates a framework aimed at achieving this. The framework provides a means to compare AGB maps with AGB estimates from a global collection of National Forest Inventories and research plots that accounts for the uncertainty of plot AGB errors. This uncertainty depends strongly on plot size, and is dominated by the combined errors from tree measurements and allometric models (inter-quartile range of their standard deviation (SD) = 30-151 Mg ha⁻¹). Estimates of sampling errors are also important, especially in the most common case where plots are smaller than map pixels (SD = 16-44 Mg ha⁻¹). Plot uncertainty estimates are used to calculate the minimum-variance linear unbiased estimates of the mean forest AGB when averaged to 0.1°. These are used to assess four AGB maps: Baccini (2000), GEOCARBON (2008), GlobBiomass (2010) and CCI Biomass (2017). Map bias, estimated using the differences between the plot and 0.1° map averages, is modelled using Random Forest regression driven by variables shown to affect the map estimates. The bias model is particularly sensitive to the map estimate of AGB and tree cover, and exhibits strong regional biases. Variograms indicate that AGB map errors have map-specific spatial correlation up to a range of 50-104 km, which increases the variance of spatially aggregated AGB map estimates compared to when pixel errors are independent. After bias adjustment, total pantropical AGB and its associated SD are derived for the four map epochs. This total becomes closer to the value estimated by the Forest Resources Assessment every after epoch and shows a similar decrease. The framework is applicable to both local and global-scale analysis, and is available at <https://github.com/arnanaraza/PlotToMap>. Our study therefore constitutes a major step towards improved AGB map validation and improvement.

Keywords: AGB, Carbon cycle, Map validation, Uncertainty assessment, Remote sensing

1. Introduction

Above-ground biomass (AGB) is the total mass of material stored in the living stems, branches and leaves of vegetation, and is often described as a biomass density, with units of mass per unit area. AGB is recognised by Global Climate Observing System (GCOS) as an Essential Climate Variable (ECV), primarily because it is intimately related to both emissions of CO₂ to the atmosphere arising from Land Use Change and fire, and uptake of CO₂ from the atmosphere due to vegetation growth (GCOS, 2016). However, it has much wider significance because of its value to human societies for energy, materials and other ecosystem services, and is also important in forest management and for policy initiatives such as Reducing Emissions from Deforestation and forest Degradation (REDD+). As a result, there have been major efforts to map forest AGB using Earth Observation (EO) data (Herold et al., 2019); at least 15 AGB maps for five epochs have been derived at pan-tropical to global scales according to meta-analyses by Rodríguez-Veiga et al. (2017) and Zhang et al. (2019).

Further maps are anticipated because of new missions dedicated to measuring forest structure and AGB, including the Global Ecosystem Dynamics Investigation (GEDI) LiDAR mission (Dubayah et al., 2020), the NASA-ISRO Synthetic Aperture Radar (NISAR) (Kellogg et al., 2020) and BIOMASS satellite (Quegan et al., 2019).

Current AGB maps were derived using different methods and data sources (Langner et al., 2014; Rodríguez-Veiga et al., 2017; Mitchard et al., 2013; Réjou-Méchain et al., 2019). This leads to significant disagreements between them that reduce their value for estimating carbon stocks in global and national applications. In addition, the maps have specific, individual error properties, rendering them unreliable for biomass change analysis, despite representing different epochs (Herold et al., 2019).

The accuracy of AGB estimates is normally quantified by characterising their error, i.e., the difference between the estimated and true AGB; this is normally unknown unless trees are destructively harvested to obtain their true weight. Ideally, the full error distribution would be known, but accuracy is commonly described statistically using various moments of the error distribution. Often, only two moments of the error are considered: the bias, which is the mean value of the

32 error, and the precision, which quantifies the spread in the distribution of random errors around
33 this mean (Dieck, 2007). These random errors are often less troublesome since their dispersion can
34 be reduced by averaging, but this does not reduce bias.

35

36 There are many potential sources of bias in AGB estimation, including methodological, human
37 and equipment biases when measuring tree dimensions; the use of incorrect allometric models when
38 estimating tree AGB from these measurements; factors affecting EO signals such as saturation at
39 high biomass, and mixed soil and vegetation components influencing signals from low biomass areas
40 (Réjou-Méchain et al., 2019); and variations in the EO signal due to environmental effects such
41 as rain and snow (Santoro et al., 2015). As a result, a consistently observed pattern in current
42 AGB maps derived from space data is overestimation of low biomass and underestimation of high
43 biomass (Réjou-Méchain et al., 2019; Rodríguez-Veiga et al., 2019).

44

45 Assessment of the accuracy of an AGB map has to take into account both errors in the map
46 itself and in the reference data used to validate it (Duncanson et al., 2021). Reference data are
47 commonly in situ plot measurements (plot data), whose uncertainty can be quantified using meth-
48 ods described in the Committee for Earth Observing Satellites (CEOS) AGB validation protocol
49 (Duncanson et al., 2021). Plot uncertainties originating from tree measurements have rigorously
50 been assessed at local scales (McRoberts et al., 2016; Chave et al., 2004; Harmon et al., 2015;
51 Réjou-Méchain et al., 2017), and their propagation into AGB maps has been assessed at local
52 (Chen et al., 2015) and regional scales (Rodríguez-Veiga et al., 2016). At larger scales, Avitabile
53 and Camia (2018) accounted for both plot and map uncertainties in four pan-European maps using
54 independent plot data to evaluate map bias and precision.

55

56 Consistent accuracy and uncertainty assessment of continental and global scale AGB maps are
57 hampered by the lack of a global reference dataset (Schimel et al., 2015; Rodríguez-Veiga et al.,
58 2017). Sampling the world’s forests is highly labour-intensive and expensive, and forest inventory
59 data are often not open access. National Forest Inventories (NFIs) have been established only in a
60 limited set of countries, of which a minority are in tropical areas (McRoberts and Tomppo, 2007).
61 In addition, NFIs in the tropics are often incomplete or unrepresentative because forest regions may
62 be remote, inaccessible, or located in conflict areas. Efforts have recently started to centralize and
63 standardize AGB plot data. The Forest Observation System (FOS) provides access to thousands

64 of plot data (Schepaschenko et al., 2019), and the standardization of plot data from large plots and
65 LiDAR-derived transects has been advocated (Chave et al., 2019). Other data sources, such as the
66 Global Forest Biodiversity Initiative (GFBI) (Liang et al., 2016), provide data to researchers by re-
67 quest and GFBI also encourages the contribution of data. Fine-resolution AGB maps from LiDAR
68 can also be used as an alternative to plot data for AGB map validation (McRoberts et al., 2019a)
69 and provide high-quality AGB estimates over more extended areas than forest inventories (Labriere
70 et al., 2018). Nevertheless, there are only a few fine-resolution AGB maps, open access data sources
71 and proprietary plot data that can be used under data-use agreements. The consequent lack of
72 a consistently sampled reference AGB dataset has consequences for statistical inference, which is
73 only possible under certain assumptions and requires the data to be accompanied by uncertainty
74 estimates (de Bruin et al., 2019; McRoberts et al., 2020; Duncanson et al., 2021).

75
76 Using a collection of plot datasets with uncertainty estimates across the globe offers several
77 opportunities. Firstly, differences between plot measurements and global AGB maps can reveal
78 regional patterns that may be explainable by environmental and/or ecological variables (de Bruin
79 et al., 2019). This would allow these differences to be predicted using model-based approaches. For
80 example, Tsutsumida et al. (2019) identified geographical areas with high AGB errors, attributing
81 error hotspots to local land-use practices. Secondly, global data can be used to investigate bias and
82 develop bias reduction methods. As examples, Xu et al. (2016) and Zhang and Liang (2020) ap-
83 plied random forest regression to model and remove AGB map bias, whilst Avitabile et al. (2016)
84 combined weighted linear averaging with bias removal methods when fusing the Saatchi et al.
85 (2011b) and Baccini et al. (2012) pantropical maps. Thirdly, the availability of plot-level uncer-
86 tainties allows evaluation of the extent to which plot-map differences can be attributed to map error.

87
88 A key GCOS principle for climate monitoring is that random errors and time-dependent biases in
89 satellite observations and derived products should be identified (GCOS, 2016), and more generally
90 map users prefer AGB maps to be unbiased and to have spatially explicit uncertainty information
91 (Quegan and Ciais, 2018). The latter should include information on the spatial correlation of
92 map errors since this is needed to model the precision of AGB estimates derived by averaging and
93 summing map pixel values at coarser grids or countries (de Bruin et al., 2019). In this paper, we
94 propose a model-based framework designed to meet these needs using a global opportunistic sample
95 of plot data to assess four AGB maps. This allows four questions to be addressed: (1) What is the

96 error contribution from different plot error sources? (2) How can map bias be assessed? (3) How
97 can map users and producers benefit from this framework? (4) How can the framework be applied
98 to derive the total AGB and its uncertainty in the pantropics in different periods?

99 **2. Materials and Methods**

100 *2.1. A framework for comparing plot and map estimates of AGB*

101 The framework first pre-processes plot data to minimise forest area (where “forest” is set to be
102 30-m pixels with >10% tree cover (Hansen et al., 2013)) and temporal mismatches with the AGB
103 maps (section 2.2), and then has three main analysis steps highlighted in Fig. 1. Although plot
104 estimates of AGB may be biased if an incorrect allometric model is used, this bias will tend to be
105 small if local allometric models are used, as is often the case for NFIs and research plots (Chave
106 et al., 2014). Hence we here assume they are unbiased and, after quantifying their uncertainties
107 (section 2.3), use them to calculate the minimum-variance linear unbiased (MVLU) estimates of
108 the mean AGB within 0.1° grid cells, together with their uncertainties (section 2.4). This allows
109 the biases in the maps to be quantified. Map bias and the spatial correlation of random map errors
110 are then modelled, respectively using spatial covariates and variograms of AGB residuals as inputs
111 (section 2.5), and applied to four global AGB maps (Baccini, GEOCARBON, GlobBiomass and
112 CCI Biomass; see section 2.2). Finally, we estimate the total pantropical AGB for each map epoch,
113 together with their confidence intervals, and compare them with the values from the 2020 Forest
114 Resource Assessment (UN-FAO, 2020) (section 2.6).

115

116 *2.2. Data inputs*

117 Three types of input data are needed to implement the framework: (1) plot estimates of AGB,
118 which we refer to as plot data; (2) plot data with tree-level measurements (at least tree diameter),
119 referred to as plots with tree data; and (3) global AGB maps.

120 *Plot data*

121 We used a global collection of plot data from NFIs (often derived using systematic sampling)
122 and research network plots; the latter were mainly in the tropics, where they make up a quarter of
123 the tropical plots. Most plot data were obtained under data-use agreements (see Table S1 for the
124 plot metadata). From them, we selected a subset meeting the following criteria. Plots should:

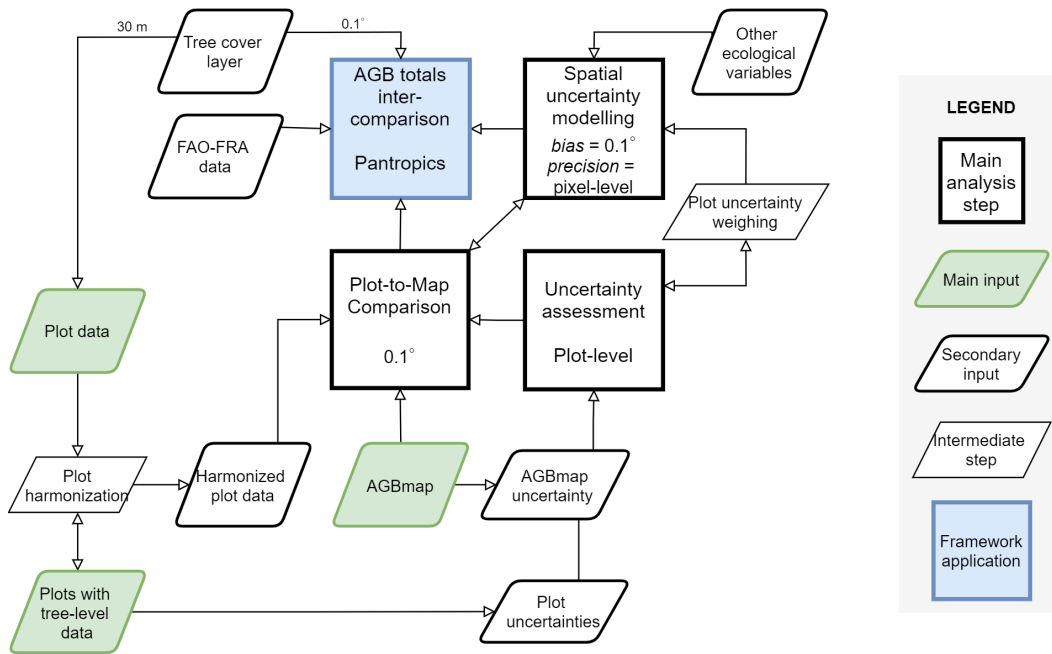


Fig. 1 Schematic of the framework indicating the three main inputs and three analysis steps leading to the comparison between plot and map estimates of AGB and the totals of the latter. Note the two-way link between the plot-to-map comparison and uncertainty modelling, indicating the assessment of map accuracy.

- 125 1. not have been used for AGB map calibration;
- 126 2. have precise coordinates to at least four decimal places in decimal degrees;
- 127 3. have been measured within ten years of the map epoch (McRoberts et al., 2015);
- 128 4. have plot-level AGB estimated using all trees with a diameter at breast height (DBH) of 10
- 129 cm or greater;
- 130 5. not have been deforested in the period between the inventory and the map epoch, according
- 131 to forest loss data (Hansen et al., 2013);
- 132 6. have comprehensive metadata that contains information about field measurement, allometric
- 133 model and sampling scheme used;
- 134 7. have an associated report or other publication.

135 This yielded a total of at most 116,181 (out of a possible 225,698) globally distributed plots to
 136 be used as reference data. Their coverage was assessed against: (a) world regions and tree cover;
 137 (b) biomes defined by specific precipitation and temperature regimes (Iremonger and Gerrand,
 138 2011); (c) strata derived from tree cover and population density, in order to assess plot coverage
 139 in forests with and without human disturbance (Fig. 2). The plot data cover all biomes (though
 140 some, such as portions of boreal and tropical rainforest, are under-represented) and they extend

141 over all the population density and tree cover strata.

142

143 The size of individual plots ranges from 0.02 ha to 25 ha, with a median size of 0.20 ha, and
144 they cover a total area of 18,192 ha. The plot measurements took place between 1996 and 2018,
145 and their AGB values were estimated using allometric models deemed appropriate for their forest
146 area by the data providers. The mean plot AGB is 100.70 Mg ha⁻¹ with a standard deviation (SD)
147 of 158.31 Mg ha⁻¹. More comprehensive plot summary statistics are shown in Table S2.

148

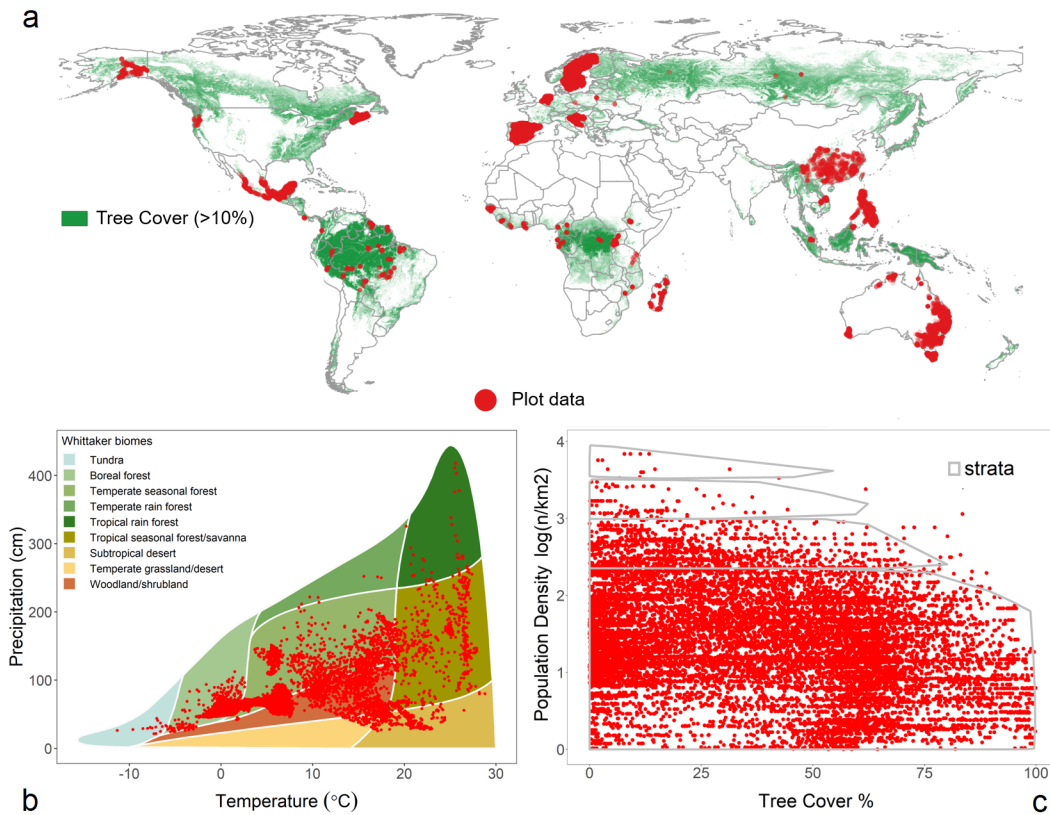


Fig. 2 Distribution of the plot data: (a) within countries and areas with > 10% tree cover (Hansen et al., 2013); (b) within ecological regions or biomes (Whittaker, 1975) as a function of rainfall and temperature; (c) within strata with and without possible man-made forest disturbances as indicated by a scatterplot of log₂-scaled human population density (Balk and Yetman, 2004) against tree cover percentage.

149 *Harmonizing plot and map data*

150 Comparisons between plot and map data are only meaningful if they share common spatial
151 and temporal characteristics. This requires applying two pre-processing steps to the plot data.
152 For plots surveyed either before or after the map epoch, the first uses forest growth data and the

153 number of years between the plot and map estimates to adjust the plot AGB to the date of the map
154 data (Avitabile and Camia, 2018). We used the growth data from model-based estimates derived
155 from chronosequences and permanent plots for the tropics and subtropics (Suarez et al., 2019), and
156 for temperate and boreal regions (Buendia et al., 2019); these are improvements of the estimates
157 in the IPCC 2006 report. Specific growth data are used depending on the forest type, ecological
158 region, forest age and continent. The second step deals with the different areas of the forest plots
159 and the AGB map support unit (i.e., the original pixel size or a coarser grid cell). Note that the
160 map provides an estimate of AGB within each support unit, but this may include non-woody and
161 non-forest areas, especially in heterogeneous and fragmented landscapes (Chave et al., 2004; Nasci-
162 mento and Laurance, 2002). AGB maps including non-forest woody vegetation are also preferred
163 by some users, including climate modellers (Quegan and Ciais, 2018). To provide an estimate of
164 the same quantity from plot data, we assume that the plot data properly represent the forested
165 part of the support unit and other types of land cover have negligible AGB. Then for plots smaller
166 than the support unit, the plot-based estimate of the AGB in the support unit (or average AGB for
167 coarser grid cells) is given by multiplying the plot AGB by the forest fraction (0-1), where this is
168 derived by defining forests as areas with at least 10% tree cover (following Food and Agriculture Or-
169 ganization guidelines (UN-FAO, 2010)) and using the 30-m tree cover layer by Hansen et al. (2013).

170

171 *AGB maps*

172 From the AGB maps listed in Table S3, four were selected on the basis of three criteria: (1)
173 global extent; (2) open access; (3) accompanying maps of uncertainty (referred to as an SD layer).
174 The Baccini map (epoch 2000), is based on the two-step method of Baccini et al. (2012) that first
175 establishes a statistical model relating spaceborne LiDAR metrics to AGB reference plots, allowing
176 AGB estimation at the LiDAR footprints. These AGB estimates are then used to calibrate a sta-
177 tistical model which estimates AGB from Landsat reflectance, thus generating a global AGB map
178 accessible at <https://www.globalforestwatch.org/>. The available SD layer of the Baccini map in-
179 cludes estimates of errors from allometric models, the LiDAR-based model and the Landsat-based
180 model, and is currently limited to the pantropics, but the provision of the global layer on the Global
181 Forest Watch platform is planned (Table S3). The GEOCARBON 2007-2010 map (Avitabile et al.,
182 2014) was produced by combining a refined pantropical map (Avitabile et al., 2016) (a fusion of
183 the Saatchi et al. (2011b) and Baccini et al. (2012) maps) with the boreal map of Santoro et al.

184 (2015), to obtain global coverage. The SD layer of the refined pantropical map is estimated using a
185 procedure based on error stratification, whereas that of the boreal map accounts for random varia-
186 tion in the radar backscatter intensity used to predict growing stock volume (GSV) and AGB. The
187 GlobBiomass 2010 and the CCI Biomass 2017 version 1 maps were produced from spaceborne syn-
188 thetic aperture radar (SAR) images of backscattered intensity (Santoro and Cartus, 2019; Santoro
189 et al., 2020), from which GSV was estimated using physically-based models and then converted to
190 AGB by scaling for wood density and biomass expansion factors estimated from empirical models
191 (Santoro et al., 2020). The SD layers of the two maps account for random errors in radar data and
192 from the biomass retrieval process and its parameters using a first-order Taylor series approach.
193 The Baccini and GEOCARBON maps are limited to forest areas, while GlobBiomass and CCI
194 Biomass maps include non-forest areas.

195

196 *2.3. Uncertainty in estimating AGB from plot data*

197 The plot harmonization described in section 2.2 involves adjusting plot values to minimize tem-
198 poral and areal mismatches between the plot and map estimates, both of which involve uncertainty.
199 Another cause of difference between the true AGB in a map pixel and its estimate from plot data
200 comes from sampling errors since plots are typically smaller than map pixels (Baccini et al., 2007).
201 This section describes the methods used to estimate the SDs of these error sources.

202

203 *Plot measurement and allometric model errors*

204 Non-destructive forest inventory is the traditional method used to estimate tree AGB, but has
205 an uncertainty of 5-44% at the stand scale (Burt et al., 2020). Tree measurement errors originate
206 from uncalibrated surveying tools and human errors, which propagate into the allometric model
207 used to estimate AGB from tree diameter (and height) per tree, and then into aggregation at plot-
208 level (Réjou-Méchain et al., 2017). The cumulative error from tree measurement and allometric
209 models is termed “measurement error” in this study.

210

211 To estimate the uncertainty in measurement errors (SD_{me}), plots with tree data were used to
212 estimate how errors in individual tree measurements propagate into biomass estimates at plot-level.
213 We used data from 8,457 plots, ranging from 0 to 25 ha in size and with a total of 267,907 trees.

214 These plots are within all the major climatic zones (tropics, sub-tropics, temperate and boreal)
215 and across eight countries, of which the majority are in the tropics. However, plots with tree data
216 constitute only 7.4% of all plot data used in our analysis. A two-step approach was therefore
217 implemented to predict SD_{me} for all plots using a model calibrated on the plots with tree data.

218

219 The first step estimated tree-level errors due to uncertainty in tree parameters (wood density,
220 diameter and tree height). Tree wood density data and their uncertainty were obtained from
221 global and regional databases (Chave et al., 2009). For trees without height data, stem diameter
222 was used to estimate height, H , using the Weibull height-diameter model (equation 1). This
223 three-parameter estimator of H has been tested within tropical forests (Feldpausch et al., 2012),
224 temperate coniferous forests in Norway (Mahanta and Borah, 2014) and China (Zhang et al., 2014),
225 boreal forests (Zhang et al., 2018), and coniferous forests in the Philippine Highlands (Anacioco
226 et al., 2018):

$$H = a(1 - \exp(-(DBH/b)^c)) \quad (1)$$

227 where DBH is diameter at breast height and a , b and c are fitted coefficients.

228

229 Errors arising from the parameters in the biomass allometric model, such as model coefficients
230 and residual standard errors, were also considered. These data are derived from the dataset of de-
231 structive tree measurements provided in Chave et al. (2014). The overall error propagation included
232 the probability distributions of the tree and allometric model parameters and was implemented
233 by running 1000 Monte Carlo simulations using the *AGBmonteCarlo* function of the *BIOMASS R*
234 package (Réjou-Méchain et al., 2017). The outputs are estimates of AGB and its SD_{me} for each
235 tree, which were aggregated to plot-level.

236

237 In the second step, a random forest (RF) model trained on the SD_{me} of the 8,457 plots using
238 climatic zones, AGB and plot size as covariates was used to predict SD_{me} for all plots. The RF
239 model predictions were tested using an independent random subset containing a third ($n=2,819$)
240 of the plots with tree data. The evaluation of the model resulted in an R^2 of 0.86 and Root Mean
241 Square Error (RMSE) of 22.1 Mg ha^{-1} .

242

243 *Temporal differences*

244 The correction for plot and map temporal mismatch introduces errors caused by uncertainties
245 in the growth rate, for which data are available per forest type, biome and continent. To derive
246 the temporal uncertainty for the plots, SD_{td} , we multiplied the SD of the growth data in Table
247 4.9 of IPCC 2019 (Buendia et al., 2019), SD_{gr} , in $Mg\ ha^{-1}\ yr^{-1}$, by the difference between the plot
248 survey year (PY) and the map epoch (MY):

$$SD_{td} = SD_{gr} * |MY - PY| \quad (2)$$

249 *Sampling error*

250 The sampling error can be significant, especially when the AGB exhibits large local variability
251 since plots are often smaller than map pixels (Baccini et al., 2007). To estimate this within-pixel
252 sampling error, spatial configurations using measured data from 8-60 ha plots and 5-250 m EO
253 footprints were simulated by Réjou-Méchain et al. (2014). For each simulation, configurations of
254 both plot and pixel were randomly located. For simulations where plots are smaller than pixels,
255 the RMSE was computed and normalized by the mean AGB of the footprint to derive a Coefficient
256 of Variation (CV).

257

258 We adopted the results of Fig. 6 and Table S2 of Réjou-Méchain et al. (2014) to train an RF
259 model to predict CV as a function of plot size and AGB map pixel size. We evaluated the model
260 using one-third of the total set of plots ($n=38,289$) which yielded an R^2 of 0.81 and an RMSE of
261 0.07. The CV was then converted into the SD of sampling error (SD_{se}) by multiplying by the mean
262 AGB of all the plot data ($\bar{\mu}AGB$) (equation 3).

$$SD_{se} = \bar{\mu}AGB * CV \quad (3)$$

263 *Plot-level uncertainty*

264 Assuming the three error sources are independent, the uncertainty in the estimate of the mean
265 AGB within a map pixel using plot data, SD_p , is then given by:

$$SD_p = \sqrt{SD_{me}^2 + SD_{td}^2 + SD_{se}^2} \quad (4)$$

266 The SDs of the three main plot error sources and the maps were analyzed for each map over
267 three groups of plot sizes: large plots (1-25 ha), plots of moderate size (0.3-1 ha) and smaller plots,
268 usually from NFIs (<0.3 ha); and over biomass ranges (<150, 150-300, and >300 Mg ha⁻¹). The
269 same grouping was also used to summarize the SD layers of the maps.

270

271 *2.4. Comparison of plot and map estimates of AGB*

272 *Aggregation to 0.1° grid cells*

273 The plot data were compared with the AGB maps in 0.1° grid cells (referred to below as
274 default AGB maps), which is a spatial scale comparable to those typically used in global carbon
275 cycle and climate models. Non-forest pixels (taken to have AGB = 0) were included for Baccini and
276 GEOCARBON prior to aggregation to avoid biasing the 0.1° AGB averages if only forest pixels
277 are used. For each grid-cell i , its average AGB was estimated from the map data by averaging
278 the AGB estimates at each pixel in the cell; and from the plot data by the MVLU estimate under
279 the assumption that the plot data are unbiased. The MVLU estimate is the weighted sum of each
280 plot estimate of AGB, x , inside the grid cell i , where the weight is inversely proportional to the
281 variance of x . Hence the plot-based estimate of the AGB of the grid cell has uncertainty $SD_{pG}(i)$
282 given by equation (5), where the summation is over all plots in the grid cell.

$$SD_{pG}(i) = \sqrt{1 / \sum (1 / SD_p^2(x))} \quad (5)$$

283 Only grid cells containing at least 5 plots were selected; on average these cells contained 15
284 plots, with an average total area of 2.3 ha. Around 46% of the total number of available grid cells
285 were excluded from this selection process. Similar studies have also set minimum plot numbers to
286 select grid cells for map assessment, e.g., Fazakas et al. (1999); Baccini et al. (2012, 2017); Xu et al.
287 (2021). Although in some cases these plots may not properly represent the grid cell, notably when
288 they are research plots lying in particular types of forest, only 4% globally and 24% of the tropical
289 plots used for analysis are research plots. This issue is discussed further in section 4.3, and Figs.
290 S1 and S2.

291 *Evaluation of differences between plot and map estimates of AGB*

292 Plot and map estimates of AGB were tabulated and compared in AGB bins of width 50 Mg
293 ha⁻¹. For each bin, the following accuracy metrics were computed: Root Mean Squared Difference

294 ($RMSD$) between map and plot AGB at 0.1° (AGB_{mG} and AGB_{pG}) for all grid cells within the
 295 bin (n) (equation 6); and the Mean Difference MD (equation 7), which is interpreted as map bias
 296 or simply “bias”. Scatterplots were also used to locate transitions from map overestimation to
 297 underestimation and AGB ranges exhibiting little bias. The scatterplots have a higher number of
 298 AGB bins than the tabulated results.

$$RMSD = \sqrt{\sum_{i=1}^n \frac{(AGB_{mG}(i) - AGB_{pG}(i))^2}{n}} \quad (6)$$

$$MD = (\bar{\mu}AGB_{mG} - \bar{\mu}AGB_{pG}) \quad (7)$$

301 *Map error conformity*

302 We assessed whether the reported map SD is consistent with the plot SD and the other uncer-
 303 tainty components at 0.1° using a metric denoted as map error conformity (EC). Map uncertainty
 304 is classified as optimistic (OP) or pessimistic (PE) according to equation 8.

$$EC = \begin{cases} OP & \text{if } (\bar{\mu}SD_{mG}^2) \leq RMSD^2 - MD^2 - (\bar{\mu}SD_{pG}^2) \\ PE & \text{otherwise} \end{cases} \quad (8)$$

308 *2.5. Spatial uncertainty*

309 This section details the model-based approach to predicting bias and the geostatistical approach
 310 to modeling precision when aggregating map SD over the tropics. The restriction to the tropics
 311 is because the extra-tropical SD layer is not currently available for the Baccini map (section 2.2),
 312 and since most plots with tree-level data used for measurement error estimation are in the tropics.

314 *The Random Forest algorithm*

315 We used RF (Breiman, 2001) to model and predict bias. RF is a non-parametric ensemble
 316 model of decision trees from bootstrapped samples of the training data and produces averaged
 317 predictions (RF regression). We implemented RF using the *ranger R* package (Wright and Ziegler,

2017). This provides a standard error (SE) of the RF model, calculated using the infinitesimal jackknife approach (Wager et al., 2014) along with a function *case.weights* that prioritizes data with higher weights when forming the bootstrap samples, and hence the trees of the RF model.

321

322 *Bias modelling*

323 We modelled bias using RF regression and data at 0.1° to form weighted bootstrap samples.
324 The model used open access sources of spatially exhaustive covariates that were considered to have
325 a possible influence on bias (Chave et al., 2004; Réjou-Méchain et al., 2014; Santoro et al., 2015),
326 all averaged to 0.1° . We first tested 10 covariates, including the AGB map itself, its reported un-
327 certainty, slope, aspect, tree cover, elevation, rainfall, temperature, biomes, longitude and latitude.
328 Using all and partial combinations of the covariates, we created multiple RF models using the
329 default RF hyperparameters. The models were evaluated using a randomly held-out 30% of the
330 0.1° data to assess the proportion of the variance of residuals explained by the model. We then
331 visually inspected the bias for indications of geographic correlation among covariates, as suggested
332 in Meyer et al. (2019). After this initial investigation, we limited the covariates to the five listed
333 in Table 1, which also gives brief metadata on the final covariates.

334

335 The predictive power of the covariates in the RF model was assessed by the Variable Impor-
336 tance Measure (VIM) and Partial Dependence Plots (PDP). VIM is the mean decrease in accuracy
337 of an RF model after data permutation of a covariate, while a PDP shows the marginal effect
338 of covariates on bias prediction. We normalized and ranked the VIM for every AGB map. The
339 PDPs are displayed as matrices, color-coded with bias and with the axes labelled by the values of
340 a covariate pair, e.g., bias plotted against AGB map and tree cover.

341

342 Under the assumption that the error in the estimated bias is normally distributed, we derived
343 the 95% confidence intervals (CI) of the predicted bias (\widehat{MD}) using the SE from the RF model
344 (equation 9). The estimated bias was then subtracted from the default 0.1° AGB map at all grid
345 cells where the 95% CI of bias does not include zero. The corrected AGB maps (referred to as
346 bias-adjusted) were then compared with the plot estimates at 0.1° using a third of the total grid
347 cells independent from the data used for bias modelling.

348

$$95\%CI = \widehat{MD} \pm 1.96 * SE \quad (9)$$

Table 1 Covariates used in bias modelling, with a brief description, unit and spatial resolution.

| Covariates | Label | Data description | Data unit | Original spatial pixel size (m) |
|-----------------------|-------|--|---------------------|---------------------------------|
| AGB map | AGB | The AGB maps according to Baccini, GEOCAR-BON, GlobBiomass, and CCI Biomass | Mg ha ⁻¹ | 30,1000,100,100 |
| Map uncertainty layer | SD | SD of propagated errors from RS inputs and biomass model parameters when predicting AGB _{map} | Mg ha ⁻¹ | 30,1000,100,100 |
| slope | SL | Terrain steepness computed from SRTM v4.1 (Jarvis et al., 2008) ¹ using the Horn 1981 algorithm suited for rough terrain | % rise | 30 |
| aspect | ASP | Orientation of slope with respect to compass direction | degrees | 30 |
| tree cover | TC | Tree cover percentage. Source data varies between maps: Baccini = TC2000-GFC; GEOCARBON and GlobBiomass and CCI Biomass = TC2010-GFC | 1-100 | 30,30,30 |

¹Used GTOPO30 (GTOPO30-global, 2002) for latitudes over 60 degrees north

349 *Uncertainty of the aggregated AGB map over the tropics*

350 Model-based inference (as used in this study) has to account for spatial correlation in map
351 errors when summing or averaging over an area. Furthermore, the variance of map errors may vary
352 over space (heteroscedasticity). To account for the latter, the AGB residual, $AGB_R(x)$, defined
353 as map-plot difference at plot location x , was scaled by the map SD; this assumes the SD of the
354 residuals is proportional to the map SD at that point (equation 10):

$$SR(x) = \frac{AGB_R(x)}{SD_m(x)} \quad (10)$$

355 where $SR(x)$ is the scaled residual and $SD_m(x)$ is the map SD. This scaling was assumed to trans-
356 form the residuals to homoscedasticity.

357

358 We then generated variogram models, $\gamma(h)$ in equation 11, to estimate the spatial correlation
 359 of SR at spatial lag h , where x is a plot location, and the errors are assumed to be statistically
 360 stationary:

$$\gamma(h) = \frac{1}{2} \text{Var}[SR(x) - SR(x + h)] \quad (11)$$

361 As proposed in Christensen (2011), the variograms were adjusted for the variance of plot errors
 362 by subtracting the mean SD_p/SD_m from the nugget of the variograms. Using the adjusted var-
 363 iograms, $SD_m(i)$ was computed using the covariances estimated at the original map scale within
 364 each grid cell. An identical procedure was adopted when estimating the SD in the total pantropical
 365 AGB for each map (section 3.4). This step is based on the covariances $\sigma_{i,j}$ of grid cell pairs i and
 366 j ($1 \dots n$), derived after convoluting the adjusted variograms from the original map pixel size to
 367 0.1° following the procedure of Kyriakidis (2004). These covariances of the map error component
 368 yielded the variance and hence SD of the total estimated AGB within the tropical belt (SD_{trop})
 369 (equation 12):

$$SD_{\text{trop}} = \sqrt{\sum_{i=1}^n \sum_{j=1}^n \sigma_{i,j}} \quad (12)$$

370 For each AGB map, this was transformed to a 95% CI of the subsequent pantropical AGB
 371 corresponding to each map epoch.

372

373 *2.6. Total pantropical AGB*

374 The total pantropical AGB (-25° to 25° latitude) estimated from bias-adjusted maps were com-
 375 pared to that given by the default 0.1° maps i.e., not adjusted for bias. The 2020 Forest Resource
 376 Assessment (FRA) (UN-FAO, 2020) data for 2000, 2010 and 2017 (2017 as the average of 2015
 377 and 2020) were also used to assess how AGB data compares with map estimates over time. Since
 378 the FRA provides AGB only in forest areas, we used 0.1° tree cover maps to remove 0.1° grid cells
 379 whose forest cover was less than a given threshold, chosen to produce a pantropical forest area
 380 close to that reported in the FRA. We used the Hansen et al. (2013) tree cover from 2000 for the
 381 2000 map and from 2010 for the 2010 and 2017 maps.

382

383 **3. Results**

384 *3.1. Uncertainty as a function of plot size and AGB*

385 For plots < 0.3 ha, the inter-quartile range of SD was 30-151 Mg ha⁻¹ for measurement error
 386 and 16-44 Mg ha⁻¹ for sampling error (Fig. 3). The SD of measurement error decreased sharply
 387 for larger plots and increased slightly as AGB increased. The sampling errors were also affected
 388 by map pixel size. For instance, GEOCARBON (1 km pixels) had consistently higher SD than
 389 Baccini (30 m pixels). Plots that were temporally adjusted for epoch 2000 (Baccini) and 2017 (CCI
 390 Biomass) exhibited slightly higher temporal SDs than for the other two maps because of the longer
 391 periods that had to be bridged between the map epoch and plot inventory date (Table S1), but
 392 the temporal error had the lowest SD of the three error sources. On average among the maps, the
 393 estimated SD of each error was 93.9 Mg ha⁻¹ (measurement), 51.6 Mg ha⁻¹ (sampling) and 24.6 Mg
 394 ha⁻¹ (temporal), equivalent to 73, 22 and 5% of the total variance, respectively. Map SDs exhibited
 395 very different magnitudes, but high map AGB values were always associated with higher map SD.

396

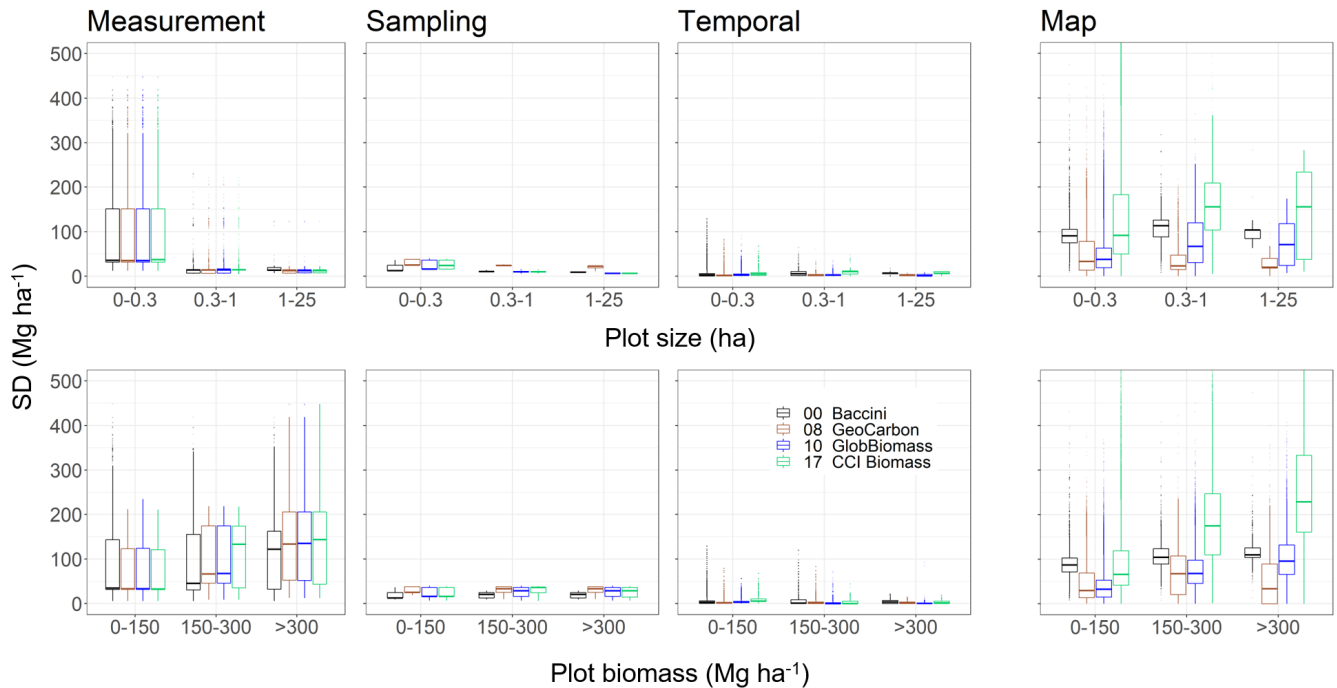


Fig. 3 Boxplots of plot-level SD for measurement error, sampling error and temporal adjustment as a function of plot size and AGB, color-coded and labelled according to the AGB map they are compared with; the horizontal bar indicates the median and the boxes show the inter-quartile range. Also depicted are boxplots of map SD as a function of plot size and AGB.

397 *3.2. Plot-to-map comparison*

398 Comparisons between map and plot estimates of AGB at 0.1° in Fig. 4 and Table 2 show that,
399 while all the maps overestimate lower biomass and underestimate higher biomass, the transition
400 point from over- to under-estimation differs. For example, the Baccini map starts to underestimate
401 AGB at around 150 Mg ha^{-1} , whereas for the other maps this occurs around 200 Mg ha^{-1} . For all
402 maps, the largest underestimation of AGB was in the highest biomass bin. GEOCARBON has
403 the smallest underestimation for values of $\text{AGB} > 300 \text{ Mg ha}^{-1}$, while the GlobBiomass and CCI
404 Biomass maps have the lowest absolute MD over the range $50\text{-}200 \text{ Mg ha}^{-1}$. The inter-quartile
405 ranges of the binned AGB map values do not overlap with the 1:1 line below 50 Mg ha^{-1} and above
406 300 Mg ha^{-1} , indicating bias dominates random errors for those bins.

407

408 The map error conformity (EC) in Table 2 shows that overall, GEOCARBON is optimistic
409 about map precision whilst CCI Biomass is pessimistic. The precision estimates for the Baccini
410 and GlobBiomass maps tend to be optimistic for low AGB and pessimistic for high AGB.

411

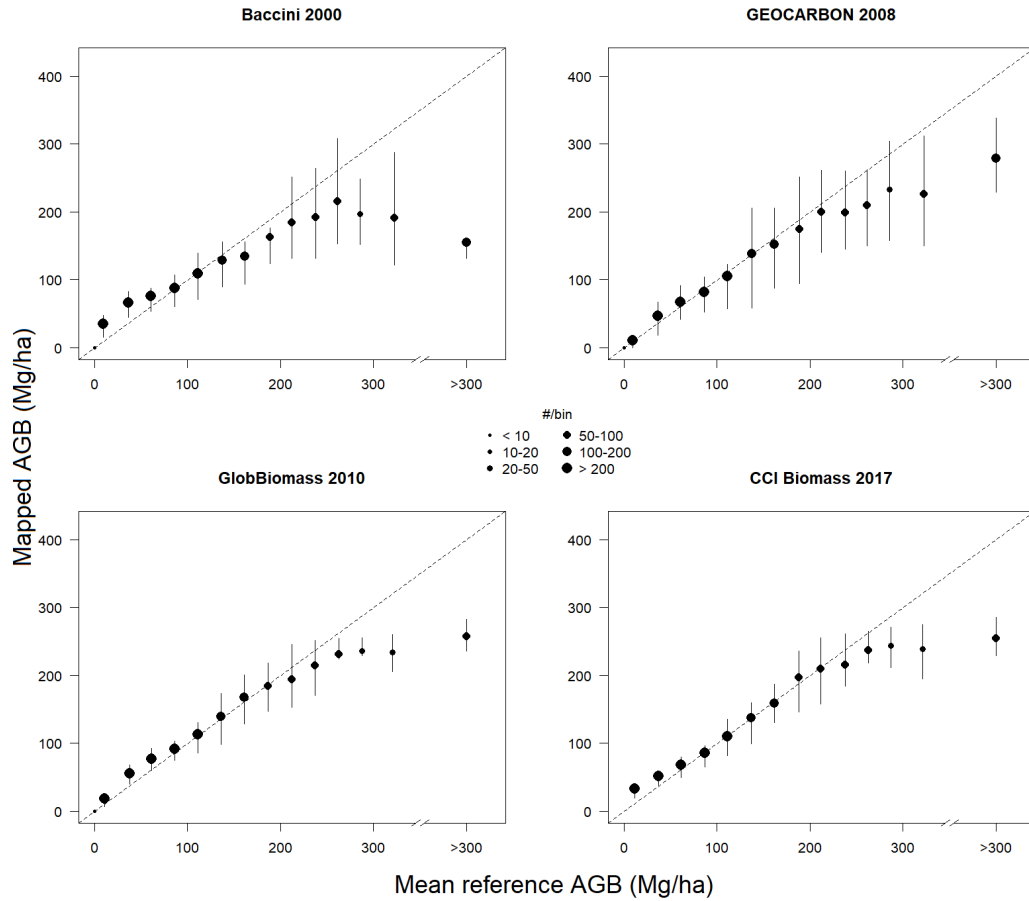


Fig. 4 Map estimates of AGB aggregated to 0.1° against mean plot AGB within 0.1° grid cells for all four AGB maps. The number of grid cells are: Baccini=6,561; GEOCARBON=6,521; GlobBiomass=6,201; and CCI Biomass=2,612 originating from plot datasets ± 10 years apart than the map epoch (see section 2.2 and Table S2). Each circle represents an AGB bin and its size denotes the number of grid cells in the bin, while the whiskers correspond to the 25th and 75th quartile range of the map AGB.

Table 2 Summary statistics of the plot-to-map comparison: mean plot and map AGB, MD (bias), RMSD, and mean variances of plot and map AGB errors per biomass bin at 0.1°. The EC column lists whether the SD layer provided with the map is optimistic (OP) or pessimistic (PE) about map precision.

| AGB bin | AGB _{pG} | AGB _{mG} | MD | RMSD | SD _{pG} ² | SD _{mG} ² | EC |
|-------------|-------------------|-------------------|-------------------------|-------|-------------------------------|-------------------------------|----|
| Baccini | ----- | ----- | - Mg ha ⁻¹ - | ----- | | | |
| 0-50 | 19 | 46 | 27 | 38 | 13325 | 6348 | OP |
| 50-100 | 69 | 80 | 11 | 45 | 27435 | 11208 | OP |
| 100-150 | 121 | 117 | -4 | 50 | 17645 | 12188 | OP |
| 150-200 | 173 | 146 | -27 | 70 | 12846 | 12976 | OP |
| 200-250 | 225 | 188 | -37 | 103 | 11849 | 14709 | PE |
| 250-300 | 270 | 209 | -61 | 109 | 11283 | 15750 | PE |
| 300-400 | 337 | 192 | -146 | 174 | 10009 | 14982 | PE |
| >400 | 793 | 147 | -647 | 761 | 33181 | 15161 | PE |
| GEOCARBON | | | | | | | |
| 0-50 | 23 | 17 | -5 | 26 | 11771 | 2221 | OP |
| 50-100 | 70 | 65 | -5 | 42 | 24989 | 8727 | OP |
| 100-150 | 121 | 122 | 1 | 80 | 20325 | 9356 | OP |
| 150-200 | 173 | 183 | 10 | 93 | 14528 | 6764 | OP |
| 200-250 | 225 | 190 | -34 | 84 | 15285 | 7334 | OP |
| 250-300 | 272 | 232 | -41 | 90 | 12224 | 3158 | OP |
| 300-400 | 338 | 287 | -51 | 105 | 20454 | 2436 | OP |
| >400 | 680 | 269 | -411 | 511 | 72987 | 131 | OP |
| GlobBiomass | | | | | | | |
| 0-50 | 23 | 35 | 12 | 22 | 11373 | 1112 | OP |
| 50-100 | 70 | 83 | 12 | 29 | 24674 | 3236 | OP |
| 100-150 | 120 | 123 | 3 | 47 | 19805 | 6188 | OP |
| 150-200 | 171 | 174 | 3 | 55 | 14042 | 9731 | OP |
| 200-250 | 225 | 205 | -20 | 59 | 14644 | 12843 | PE |
| 250-300 | 273 | 233 | -41 | 61 | 10135 | 15076 | PE |
| 300-400 | 337 | 238 | -99 | 110 | 23175 | 16465 | OP |
| >400 | 700 | 263 | -437 | 520 | 72682 | 21374 | PE |
| CCI Biomass | | | | | | | |
| 0-50 | 22 | 40 | 19 | 29 | 6845 | 13304 | PE |
| 50-100 | 72 | 75 | 3 | 31 | 21218 | 59323 | PE |
| 100-150 | 122 | 122 | -1 | 50 | 19363 | 74641 | PE |
| 150-200 | 172 | 174 | 2 | 57 | 14824 | 167434 | PE |
| 200-250 | 224 | 212 | -12 | 61 | 16401 | 211949 | PE |
| 250-300 | 274 | 240 | -34 | 58 | 9347 | 135659 | PE |
| 300-400 | 339 | 245 | -93 | 107 | 19736 | 84973 | PE |
| >400 | 680 | 253 | -426 | 503 | 71469 | 227242 | PE |

412 3.3. Spatial bias

413 The fraction of the variance of the bias explained by the RF models ranged from 24 to 36% over
414 the AGB maps. Map AGB and tree cover were the most important predictors in the models (Fig.
415 S3 and Table S4). The proportion of 0.1° grid cells for which the 95% CI of the bias prediction
416 included 0 Mg ha⁻¹ ranged from 4 to 15% across the AGB maps, so most grid cells were corrected
417 for bias.

418

419 Systematic underestimation is particularly obvious over the tropical rainforests of the Amazon,
420 the Congo basin and insular Southeast Asia (Fig. 5), but also occurs in parts of other climatic
421 zones, particularly the sub-tropical zone of China and southeast Australia, the temperate zone of
422 Spain and USA, and the boreal zone of Russia and Canada. There is no obvious common spatial
423 pattern of overestimation among the maps. The GEOCARBON map has the smallest underestima-
424 tion in the tropics, followed by the CCI Biomass map. The GlobBiomass map exhibits the largest
425 overestimation in the temperate regions, while the Baccini map has the largest overestimation in
426 the boreal zone.

427

428 3.4. Estimates of total pan-tropical AGB

429 The default and bias-adjusted maps, and the FRA all show a decrease in the total pan-tropical
430 AGB from 2000 to 2017 (Table 3), but with important differences. The bias-adjusted maps give
431 higher total AGB than the default maps for all years since they correct for map underestimation
432 in high AGB regions. The 95% CIs for the estimated total AGBs take account of the map-specific
433 spatial correlation in AGB map errors (see convoluted variograms in Fig. S5, which exhibit sills
434 from 0.11-0.38 and nugget = 0, and the modified SDs in 0.1° grid cells in Fig. S6). The differences
435 between the three estimates decrease from 2000 to 2017, though the bias-adjusted estimate is still
436 6.9 Petagrams (Pg) greater than the FRA estimate in 2017.

437

438 4. Discussion

439 4.1. Uncertainty drivers in plot-to-map comparison

440 The largest contributor to plot SD (73%) was measurement error (which includes allometric
441 model errors), which is much larger for smaller plots and increases slightly with higher biomass.

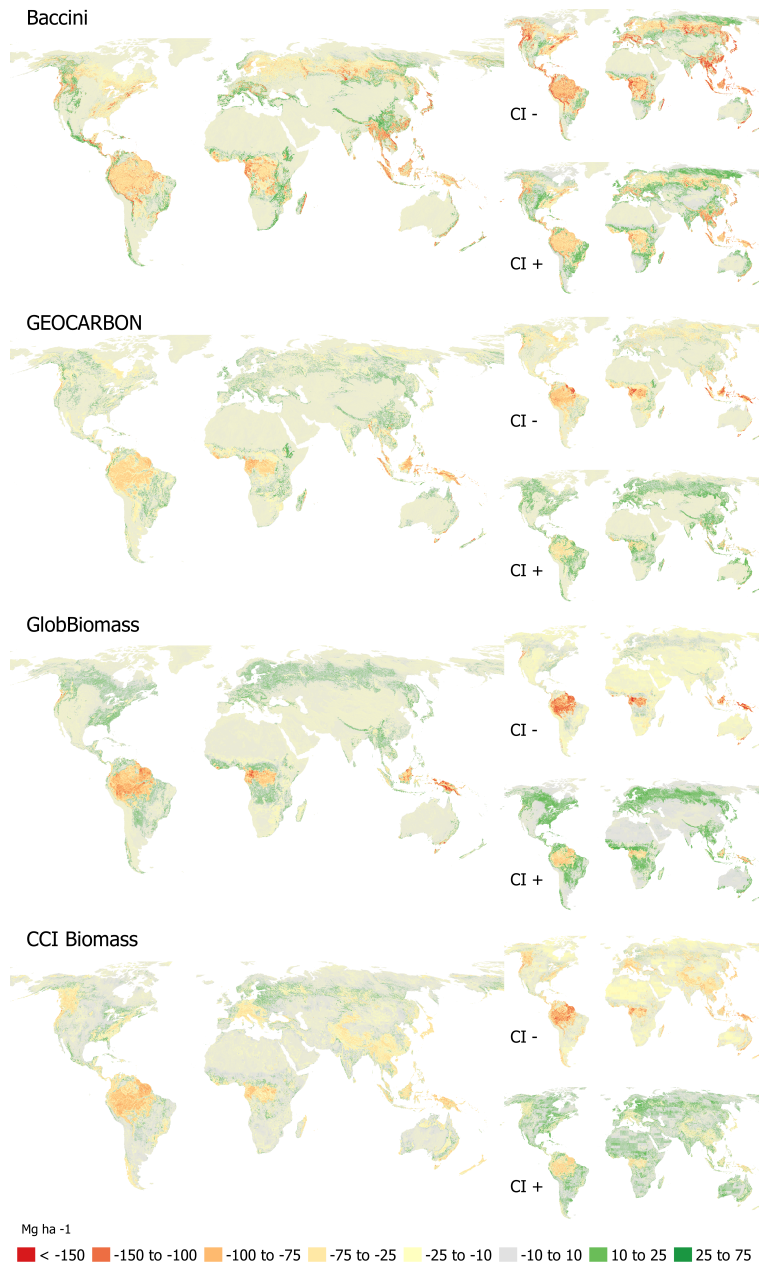


Fig. 5 The predicted bias of global biomass maps in 0.1° grid cells and their 95% CI: lower (CI-) and upper (CI+). There is a 95% chance that the bias lies within the (CI-, CI+) interval.

442 Most of the plot data come from small plots (mostly NFIs) in which there are fewer trees. Com-
 443 bined with geolocation errors causing trees near the plot boundary to be included or excluded,
 444 this produces large uncertainties (Réjou-Méchain et al., 2019). Moreover, around 34% of the plots
 445 smaller than 0.3 ha are extra-tropical, and may be subject to erroneous uncertainty estimates due
 446 to the use of the wrong allometric model (Chen et al., 2015). Generic allometric models similar to
 447 Chave et al. (2014) for non-tropical forests are not yet developed. The uncertainty of measurement

Table 3 Pantropical forest AGB with 95% CI estimated from the default and bias-adjusted maps. Also shown are estimates derived from FRA data for these three years. The forest areas of map-based AGB estimates are set as the closest possible area to the FRA forest area based on a 0.1° tree cover threshold. The analysis includes all pantropical countries but without the pantropical portions of China and Australia.

| Year | AGB (Pg) | | | Forest area (mil. ha) | | 95% CI (Pg) | |
|------|----------|------------|--------|-----------------------|---------|-------------|------------|
| | Default | This study | FRA | Map-based | FRA | Default | This study |
| 2000 | 354.47 | 406.38 | 302.69 | 1939.28 | 1998.20 | 5.83 | 0.88 |
| 2010 | 279.35 | 314.20 | 290.97 | 1928.98 | 1907.77 | 7.93 | 5.09 |
| 2017 | 277.60 | 296.20 | 283.78 | 1928.98 | 1849.50 | 14.10 | 1.57 |

448 error is probably best estimated by the data producers themselves and its provision would be a
 449 useful addition to the data quality requirements for current and upcoming plot data (see section
 450 2.2).

451

452 Sampling errors in the range $16\text{-}44 \text{ Mg ha}^{-1}$ were estimated for small plots when map pixel
 453 size and forest cover were taken into account (see section 2.2). They tend to be amplified when
 454 small plots are compared with large map pixels (Réjou-Méchain et al., 2014), as observed in the
 455 GEOCARBON results (1 km pixel size, Fig. 3), which has the highest SD for this error. This
 456 occurs partly because forest structure tends to be non-uniform over short distances (Chave et al.,
 457 2004; Saatchi et al., 2011a), especially on slopes (Réjou-Méchain et al., 2014) and when there are
 458 very big trees (de Castilho et al., 2006). However, the influence of forest structure variability tends
 459 to decrease as plot size increases, e.g., Saatchi et al. (2011a) found that the CV of sampling error
 460 was 80% smaller for 1 ha plots than for 0.01 ha plots in the tropics. As well as plot size, the
 461 number and spatial spread of plots inside a map pixel affects sampling errors (Næsset et al., 2015;
 462 Bradford et al., 2010). Several randomly placed samples may be better at capturing the mean
 463 AGB of a forest region than a single large sample covering the same total area (Nascimento and
 464 Laurance, 2002). LiDAR data may also be useful as reference data since LiDAR-based AGB maps
 465 typically cover substantial areas and hence provide samples covering the whole range of AGB in
 466 a landscape. This will prevent biases arising from preferential sampling, which is often implicit in
 467 the selection of research plots (Duncanson et al., 2021). Whenever available, these maps would be
 468 preferred over the research plots themselves as reference data.

469

470 Uncertainty from plot temporal adjustment was largest for the AGB maps of 2000 and 2017

471 because of the longer periods between the map epoch and plot inventory date (Table S1), but was
472 a small contributor to total plot uncertainty. Improvements might be possible by stratifying the
473 growth data to capture the growth of disturbed forests under different management intensities and
474 natural disturbances (Suarez et al., 2019). Such estimates could be complemented by forest age
475 maps (Besnard et al., 2021).

476

477 Map SDs exhibited very different magnitudes as a result of the use of different data, different
478 AGB estimation methods and different ways of propagating uncertainty (section 2.2). However,
479 high map AGB values are always associated with higher map SD (though not necessarily a higher
480 CV) (Rodríguez-Veiga et al., 2017). If plots are used for calibration, such as in the Baccini map,
481 large measurement errors may contribute a significant part of the total error propagated to the
482 map (Réjou-Méchain et al., 2017). AGB maps produced without in situ calibration avoid such
483 errors, but are vulnerable to model uncertainties (Santoro et al., 2011). For example, the SDs for
484 GlobBiomass and CCI Biomass arise mainly from limitations in the model converting backscatter
485 to GSV and uncertainty in its parameters (Santoro et al., 2020).

486

487 All AGB maps tended to overestimate low AGB and underestimate high AGB. Numerous stud-
488 ies, summarized in Réjou-Méchain et al. (2019) and Duncanson et al. (2021), show similar effects,
489 as a result of several intertwined factors. Both optical and radar sensors are known to saturate
490 for higher values of AGB (Zhao et al., 2016; Rodríguez-Veiga et al., 2019), which inevitably leads
491 to underestimation of AGB. However, the factors causing map overestimation for lower AGB are
492 more complex. For radar-based maps, it is largely driven by imperfect allometric models (Santoro,
493 2020) and the influence of soil moisture and roughness (Santoro et al., 2011). For maps derived
494 using optical data, it is possibly a result of fitting saturated EO data to plot data in the regression
495 models, particularly if plots are limited to certain forest conditions but used to calibrate models
496 predicting AGB globally (Rodríguez-Veiga et al., 2019). The smaller map bias in mid-range AGB
497 values is expected for regression methods, which often force the mean of the training data and pre-
498 dictions to be equal. Similar behaviour for the model-based approaches used by GlobBiomass and
499 CCI Biomass may reflect higher sensitivity of radar backscatter to AGB and reduced soil effects
500 in this AGB range. GEOCARBON has the closest match to plot data for $\text{AGB} > 200 \text{ Mg ha}^{-1}$,
501 possibly because its bias removal method used a plot dataset in the tropics which may overlap with
502 our plot data. However, this effect is not easy to quantify as here the comparison is with plot data

503 after the harmonization process (section 2.2).

504

505 *4.2. Bias and precision modelling*

506 The model-based approach to predicting bias at 0.1° yields broad-scale spatial patterns of map
507 over- and underestimation that exhibit significant similarities between the four maps (Fig. 5), and
508 are also similar to patterns observed in Avitabile et al. (2016) for two global maps and Tsutsumida
509 et al. (2019) for regional maps. Error hotspots, mainly of map underestimation, stand out in the
510 regions of agreement and disagreement between the maps (Fig. 6). Such hotspots occur regardless
511 of the methods used to produce the maps (Xu et al., 2016) whenever there are sufficient reference
512 data to compare with the maps (Avitabile et al., 2016; Rodríguez-Veiga et al., 2019). However,
513 insufficient and unrepresentative reference data may cause incorrect estimation of map bias and
514 hence erroneous map correction (Avitabile et al., 2016). We attempted to counteract this effect by
515 reducing the plot-based estimates of AGB at 0.1° when non-forest areas exist in grid cells (section
516 2.2). The plots used here cover all major ecological zones, though some zones are under-sampled,
517 and are subject to large measurement errors. These plot errors are accounted for when creating
518 the training data, as explained in section 2.5. For example, training data within areas with high
519 map underestimation, such as the Tasmanian forests, were mostly small plots, so received lower
520 weights and hence had a lower chance to become training data. A similar situation is observed in
521 Sweden.

522

523 The Variable Importance Measure (Table S4) and Partial Dependency Plots (PDP; Fig. S3)
524 indicate that the predicted bias is most sensitive to map AGB and tree cover, but this is also clear
525 from Fig. 5. In particular, the PDPs show that map underestimation of at least 60 Mg ha^{-1} mostly
526 occurs when $\text{AGB} > 300 \text{ Mg ha}^{-1}$ and canopy cover is in the range 60-90%. Furthermore, bias in
527 the radar-based maps, e.g., CCI Biomass, is sensitive to steep northeasterly slopes because of the
528 look geometry of the sensor and incorrect pre-processing of the SAR data for moderate and steep
529 terrain (Santoro and Cartus, 2019). These observations may help in developing improved AGB
530 estimators that combat such deficiencies.

531

532 Spatial autocorrelation analysis revealed spatial dependency in errors up to lags of 50-104 km,
533 depending on the map (Fig. S5). Short-range autocorrelation of residuals ($< 5 \text{ km}$) comes from

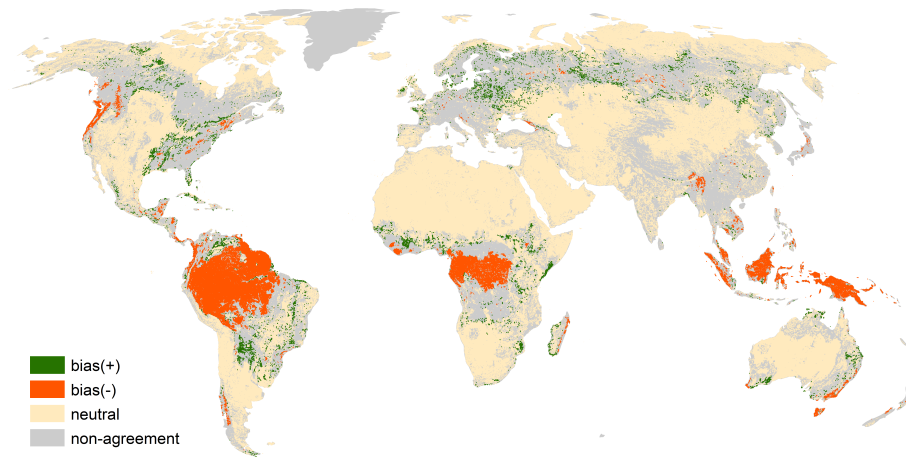


Fig. 6 Map of grid cells where the biases in the four AGB maps shown in Fig. 5 at 0.1° for 2000, 2008, 2010 and 2017 agree and disagree; overestimation or bias(+) in all maps, i.e., $10 < \text{bias} < 50$; underestimation or bias(-) in all maps, i.e., $-150 < \text{bias} < -10$; neutral in all maps, i.e., $-10 < \text{bias} < 10$. All numerical values are in Mg ha^{-1} . All other areas are in the non-agreement class.

534 localized forest structure (Guitet et al., 2015; Mascaro et al., 2014). However, longer-range auto-
 535 correlation is found from our plot data, which are mostly from NFIs that are configured to sample
 536 the forest over short distances (e.g., using nested plots) while also representing regional to country
 537 scales. Similar effects were found in other large-scale studies (Baccini et al., 2012; Avitabile et al.,
 538 2011; Ploton et al., 2020b). Large scale AGB mapping often uses environmental variables, e.g.,
 539 topography (Baccini et al., 2012) and climate (Hernández-Stefanoni et al., 2020), as predictors,
 540 and these exhibit long-range spatial dependency that may transfer into the AGB error structure
 541 (Ploton et al., 2020b). This may also affect the two radar-based maps as the GSV and biomass
 542 expansion factor used for AGB estimation are mapped with climatic variables as inputs (Santoro
 543 et al., 2020; Santoro, 2020). The variograms also indicate that the map SD layers need to be
 544 improved. In the variogram models shown in Fig. S5, the residuals are scaled by the map SD, so
 545 the SDs are incorrect when the sills deviate from 1 (see “default variogram” in Fig. S5). Further
 546 evidence for the need to adjust the SDs is given by the map error conformity measures (Table 2).
 547 Overly pessimistic estimated SD for the CCI Biomass 2017 map has already been corrected in its
 548 updated version (Santoro, 2020).

549

550 *4.3. Strengths and limitations of the framework*

551 A core GCOS principle is that estimates of AGB should as far as possible be unbiased. This
552 study provides a comprehensive framework for meeting this principle by estimating the bias and
553 uncertainty in AGB maps (Fig. 1). It can be adapted to the requirements of different map users
554 or producers (Herold et al., 2019) but requires estimates of uncertainty in both plots and maps,
555 and careful vetting of the quality and suitability of plot data. Open source tools estimating plot
556 uncertainty (e.g., *BIOMASS* and *PlotToMap*) are of great value for this. *BIOMASS* has not been
557 widely tested other than in tropical regions, though is currently being tested in extra-tropical
558 forests. We also provide an interactive online tool for users of the framework and open source
559 software (which can be readily updated) that offers more flexibility in pre-processing plot data and
560 comparing plot and map AGB estimates (<https://github.com/arnanaraza/PlotToMap>). Countries
561 with constraints on sharing plot data could use such tools while maintaining national data privacy.

562
563 Bias-adjusted maps of AGB and its uncertainty in 0.1° or larger grid cells can be used in climate
564 and carbon modelling (see Fig. S4). They can also provide estimates of national AGB over time,
565 and its uncertainty, to assist carbon accounting based on NFI sampling (McRoberts and Tomppo,
566 2007) and to enhance local AGB estimates (Næsset et al., 2020; Toan et al., 2011). In addition,
567 they can provide baseline AGB values when more frequent estimation of carbon emissions is desir-
568 able (Csillik and Asner, 2020).

569
570 Information on local to regional map biases and their dependence on terrain and forest variables
571 (Table S4, Fig. S3) may help to trace the factors causing such bias. Moreover, map producers
572 should find the analyses of spatial error structure from variograms and map error conformity in-
573 formative. For more precise maps, our variograms that account for measurement errors (i.e., with
574 zero nugget) and our optimized method of SD aggregation can be adapted.

575
576 The application of the uncertainty framework to estimating pantropical AGB showed a persis-
577 tent temporal decline in stocks and increasing agreement between the map-based estimates and the
578 estimate from FRA over time. This may reflect both increasing quality of forest AGB data from
579 countries (Nesha et al., 2021) and improving map accuracy, and suggests that we can have more
580 confidence in more recent estimates of pantropical forest AGB. However, the large disagreements
581 between the map-based and FRA estimates of AGB in 2000 indicate that long-term AGB change

582 estimation based on differences in AGB maps is likely to be unreliable. Further analysis of AGB
583 change from these estimates will be addressed in a follow-up study.

584

585 The limitations in the uncertainty framework reported here pertain to the plot dataset, plot se-
586 lection bias, methodological limitations and data requirement issues. Most plot data with tree-level
587 measurements lack tree height, so we estimated height with the Weibull model, but this model may
588 not apply in all biomes, such as woodlands and mangrove forests. We also lacked tree-level data
589 in non-tropical regions, so estimates of measurement errors for plots in these regions are subject
590 to revision. The fact that the plot dataset in the boreal regions is concentrated in two countries
591 may also limit global application of the framework.

592

593 Plot selection bias will arise if the plots inside a 0.1° grid cell do not provide a random sample
594 of the AGB within the cell. For example, if they are selected to lie within high AGB areas within
595 a diverse forest landscape, their weighted average would overestimate the AGB at 0.1° . Research
596 plots, which make up 4% of the total dataset but 24% in the tropics, are particularly prone to this
597 effect. To analyze how this might affect our analysis we examined the variability of tree cover at
598 grid scale and plot locations, and treated this as a proxy for AGB variation (Avitabile and Camia,
599 2018). This analysis yielded a set of grid cells without preferential samples (referred to as strict
600 filtering of the plot dataset; see Fig. S1 for the specific steps). Assessment of the GlobBiomass
601 map at pantropical and global scales against the filtered plot dataset (based on the tree cover for
602 the same epoch (Hansen et al., 2013)) gave results differing only slightly from use of the current
603 dataset (see Fig. S1). This suggests that preferential sampling had little effect on our analysis.
604 Possible reasons for this are that almost the same number of grid cells were excluded under the
605 current approach and the strict filter (56% and 57% in the pantropics, respectively), and that many
606 of the grid cells selected were the same under both approaches, particularly in tropical high AGB
607 areas e.g., 77% of the tropical grid cells where GlobBiomass >250 Mg ha $^{-1}$ used in the current
608 approach were also used after strict filtering (Fig. S2). Though we used several grid cells con-
609 taining research plots, these are mainly plots with area >0.60 ha located in forests that visually
610 exhibit homogeneous canopy cover. Nonetheless, the bias seen in the corrected maps when AGB
611 >300 Mg ha $^{-1}$ may be exacerbated by the lack of representative plot data, even if the minimum
612 number of plots inside grid cells is increased. This AGB range was only covered by research plots
613 in Tasmanian and Amazonian forests, and most of them were excluded from the bias modelling

614 since the weighted bootstrapping limits the use of small plots with high AGB.

615

616 A number of possibilities exist for improving the bias modelling. Using additional covari-
617 ates, such as AGB texture and canopy height, may help (Xu et al., 2021). Additional plot data,
618 preferably large plots, are desirable both to compensate for those with high variance and, more
619 importantly, to increase spatial coverage since a large training dataset is needed to capture local
620 AGB error patterns (Xu et al., 2016). Selected values from local AGB maps, if they exist, can
621 be added to the training data in under-sampled areas (McRoberts et al., 2019b). We also plan
622 to assess different cross-validations of the bias model. In addition, the use of harmonized plots at
623 coarser scales, e.g., 1 km from forestry concessions (Ploton et al., 2020a) and 25 km from NFIs
624 (Menlove and Healey, 2020) are also options, given their extensive forest coverage.

625

626 5. Conclusions

- 627 1. The comprehensive uncertainty framework developed in this paper can correct existing AGB
628 maps for bias, within the limitations of the bias model. Such maps, with their associated
629 SDs at coarser scales, are particularly useful in the context of climate and carbon cycle
630 modelling. The analysis of spatial bias and models of spatial error correlation provide valuable
631 information to both map users and producers on local to regional map errors.
- 632 2. The estimates of bias in the AGB maps exhibit spatial patterns that largely reflect AGB
633 itself. The bias models would benefit from additional plot data and local AGB maps within
634 poorly represented regions i.e., LiDAR-based maps will be preferred over plot data whenever
635 available.
- 636 3. The spatial uncertainty modelling was hindered by plot AGB uncertainty arising principally
637 from measurement and sampling errors, which tends to be especially large in regions where
638 only small plots are available. It would be helpful if NFIs included some larger plots to serve
639 multiple purposes, including the assessment of global AGB maps.
- 640 4. Both map-based and FRA estimates of pantropical AGB show a decline from 2000 to 2017,
641 and become increasingly close with time, despite the datasets and methods used being quite

642 different for different map epochs. However, there is still a difference of 6.9 Pg between the
643 map-based and FRA estimate in 2017.

644 **Acknowledgements:** This study has been partly supported by the IFBN and CCI Biomass
645 projects funded by ESA. We thank Michael Keller and Alessandro Baccini for their data provision,
646 and Maxime Rejou-Mechain and Philippe Ciais for their technical suggestions. We also thank the
647 government offices, non-government organizations and foresters behind the forest inventories. Plot
648 data from Russia was processed within the framework of the state assignment of the Center for
649 Forest Ecology and Productivity of the Russian Academy of Sciences (no.-18-118052590019-7), and
650 was financially supported by the Russian Science Foundation (project no. 19-77-30015).

651

652 **Data repository:** Access for the bias-adjusted maps and associated SDs:

653 <https://doi.org/10.6084/m9.figshare.18393689.v1>.

654

655 **Author contributions:** Araza, de Bruin and Herold conceptualized the study and analyzed
656 the results; Araza and de Bruin designed the methodology; Araza led the manuscript writing;
657 de Bruin, Quegan, Labriere and Rodriguez-Veiga provided technical contributions and text sug-
658 gestions; Avitabile and Santoro provided the AGB maps and text suggestions; Mitchard, Ryan,
659 Phillips, Wilcock, Verbeeck, Carreiras, Schelhaas provided plot data and technical suggestions;
660 Pascagaza, Bispo, Laurin, Vieilledent, Slik, Wijaya, Lewis, Morel, Liang, Sukhdeo, Schepaschenko,
661 Cavlovic, Gilani and Lucas provided data and text suggestions; Quegan proofread the manuscript;
662 Herold and Hein acquired funding and provided text suggestions. All authors contributed critically
663 to the paper and gave final approval for publication.

664 References

- 665 Anacioco, K.P., Gorio, J.A.L., Padsico, M.R.S., Lumbres, R.I.C., Doyog, N.D., Lee, Y.J., 2018.
666 Fitting and evaluation of height-diameter models for alnus japonica in la trinidad, benguet,
667 philippines. *Journal of Mountain Science* 15, 2422–2432. [https://doi.org/10.1007/s11629-018-](https://doi.org/10.1007/s11629-018-4866-9)
668 4866-9.
- 669 Avitabile, V., Camia, A., 2018. An assessment of forest biomass maps in europe using harmo-
670 nized national statistics and inventory plots. *Forest Ecology and Management* 409, 489–498.
671 <https://doi.org/10.1016/j.foreco.2017.11.047>.
- 672 Avitabile, V., Herold, M., Henry, M., Schmullius, C., 2011. Mapping biomass with remote sensing:
673 a comparison of methods for the case study of uganda. *Carbon Balance and Management* 6.
674 <https://doi.org/10.1186/1750-0680-6-7>.
- 675 Avitabile, V., Herold, M., Heuvelink, G.B.M., Lewis, S.L., Phillips, O.L., Asner, G.P., Armston,
676 J., Ashton, P.S., Banin, L., Bayol, N., Berry, N.J., Boeckx, P., de Jong, B.H.J., DeVries, B.,
677 Girardin, C.A.J., Kearsley, E., Lindsell, J.A., Lopez-Gonzalez, G., Lucas, R., Malhi, Y., Morel,
678 A., Mitchard, E.T.A., Nagy, L., Qie, L., Quinones, M.J., Ryan, C.M., Ferry, S.J.W., Sunderland,
679 T., Laurin, G.V., Gatti, R.C., Valentini, R., Verbeeck, H., Wijaya, A., Willcock, S., 2016. An
680 integrated pan-tropical biomass map using multiple reference datasets. *Global Change Biology*
681 22, 1406–1420. <https://doi.org/10.1111/gcb.13139>.
- 682 Avitabile, V., Herold, M., Lewis, S., Phillips, O., Aguilar-Amuchastegui, N., Asner, G., Brien-
683 R., DeVries, B., Gazolla Gatti, R., Feldpausch, T., Girardin, C., de Jong, B., Kearsley, E.,
684 Klop, E., Lin, X., Lindsell, J., Lopez-Gonzalez, G., Lucas, R., Malhi, Y., Morel, A., Mitchard,
685 E., Pandey, D., Piao, S., Ryan, C., Sales, M., Santoro, M., Vaglio Laurin, G., Valentini, R.,
686 Verbeeck, H., Wijaya, A., Willcock, S., 2014. Comparative analysis and fusion for improved
687 global biomass mapping. pp. 251–252. <https://colloque6.inra.fr/gv2m/Oral-Sessions>.
- 688 Baccini, A., Friedl, M., Woodcock, C., Zhu, Z., 2007. Scaling field data to calibrate and validate
689 moderate spatial resolution remote sensing models. *Photogrammetric Engineering & Remote*
690 *Sensing* 73, 945–954. <https://doi.org/10.14358/pers.73.8.945>.
- 691 Baccini, A., Goetz, S.J., Walker, W.S., Laporte, N.T., Sun, M., Sulla-Menashe, D., Hackler, J.,
692 Beck, P.S.A., Dubayah, R., Friedl, M.A., Samanta, S., Houghton, R.A., 2012. Estimated carbon

693 dioxide emissions from tropical deforestation improved by carbon-density maps. *Nature Climate*
694 *Change* 2, 182–185. <https://doi.org/10.1038/nclimate1354>.

695 Baccini, A., Walker, W., Carvalho, L., Farina, M., Sulla-Menashe, D., Houghton, R.A., 2017.
696 Tropical forests are a net carbon source based on aboveground measurements of gain and loss.
697 *Science* 358, 230–234. <https://doi.org/10.1126/science.aam5962>, [10.1126/science.aam5962](https://doi.org/10.1126/science.aam5962).

698 Balk, D., Yetman, G., 2004. The global distribution of population: evaluating the gains in resolution
699 refinement. New York: Center for International Earth Science Information Network (CIESIN),
700 Columbia University .

701 Besnard, S., Koirala, S., Santoro, M., Weber, U., Nelson, J., Gütter, J., Herault, B., Kassi, J.,
702 N'Guessan, A., Neigh, C., Poulter, B., Zhang, T., Carvalhais, N., 2021. Mapping global forest
703 age from forest inventories, biomass and climate data. *Earth System Science Data* 13, 4881–4896.
704 [10.5194/essd-13-4881-2021](https://doi.org/10.5194/essd-13-4881-2021).

705 Bradford, J.B., Weishampel, P., Smith, M.L., Kolka, R., Birdsey, R.A., Ollinger, S.V., Ryan,
706 M.G., 2010. Carbon pools and fluxes in small temperate forest landscapes: Variability
707 and implications for sampling design. *Forest Ecology and Management* 259, 1245–1254.
708 <https://doi.org/10.1016/j.foreco.2009.04.009>.

709 Breiman, L., 2001. *Machine Learning* 45, 5–32. <https://doi.org/10.1023/a:1010933404324>.

710 de Bruin, S., Herold, M., Araza, A., 2019. Product Validation Plan. Technical Report. European
711 Space Agency.

712 Buendia, E., Tanabe, K., Kranjc, A., Baasansuren, J., Fukuda, M., Ngarize, S., Osako, A., Py-
713 rozhenko, Y., Shermanau, P., Federici, S., 2019. Refinement to the 2006 ipcc guidelines for
714 national greenhouse gas inventories. IPCC: Geneva, Switzerland .

715 Burt, A., Calders, K., Cuni-Sanchez, A., Gómez-Dans, J., Lewis, P., Lewis, S.L., Malhi, Y., Phillips,
716 O.L., Disney, M., 2020. Assessment of bias in pan-tropical biomass predictions. *Frontiers in*
717 *Forests and Global Change* 3. <https://doi.org/10.3389/ffgc.2020.00012>.

718 de Castilho, C.V., Magnusson, W.E., de Araújo, R.N.O., Luizão, R.C., Luizão, F.J., Lima,
719 A.P., Higuchi, N., 2006. Variation in aboveground tree live biomass in a central amazo-

720 nian forest: Effects of soil and topography. *Forest Ecology and Management* 234, 85–96.
721 <https://doi.org/10.1016/j.foreco.2006.06.024>.

722 Chave, J., Condit, R., Aguilar, S., Hernandez, A., Lao, S., Perez, R., 2004. Er-
723 ror propagation and scaling for tropical forest biomass estimates. *Philosophical Trans-*
724 *actions of the Royal Society of London. Series B: Biological Sciences* 359, 409–420.
725 <https://doi.org/10.1098/rstb.2003.1425>.

726 Chave, J., Coomes, D., Jansen, S., Lewis, S.L., Swenson, N.G., Zanne, A.E., 2009. Towards a world-
727 wide wood economics spectrum. *Ecology Letters* 12, 351–366. [https://doi.org/10.1111/j.1461-](https://doi.org/10.1111/j.1461-0248.2009.01285.x)
728 [0248.2009.01285.x](https://doi.org/10.1111/j.1461-0248.2009.01285.x).

729 Chave, J., Davies, S.J., Phillips, O.L., Lewis, S.L., Sist, P., Schepaschenko, D., Arm-
730 ston, J., Baker, T.R., Coomes, D., Disney, M., Duncanson, L., Hérault, B., Labrière,
731 N., Meyer, V., Réjou-Méchain, M., Scipal, K., Saatchi, S., 2019. Ground data are
732 essential for biomass remote sensing missions. *Surveys in Geophysics* 40, 863–880.
733 <https://doi.org/10.1007/s10712-019-09528-w>.

734 Chave, J., Réjou-Méchain, M., Búrquez, A., Chidumayo, E., Colgan, M.S., Delitti, W.B., Duque,
735 A., Eid, T., Fearnside, P.M., Goodman, R.C., Henry, M., Martínez-Yrizar, A., Mugasha, W.A.,
736 Muller-Landau, H.C., Mencuccini, M., Nelson, B.W., Ngomanda, A., Nogueira, E.M., Ortiz-
737 Malavassi, E., Péliissier, R., Ploton, P., Ryan, C.M., Saldarriaga, J.G., Vieilledent, G., 2014.
738 Improved allometric models to estimate the aboveground biomass of tropical trees. *Global*
739 *Change Biology* 20, 3177–3190. <https://doi.org/10.1111/gcb.12629>.

740 Chen, Q., Laurin, G.V., Valentini, R., 2015. Uncertainty of remotely sensed aboveground biomass
741 over an african tropical forest: Propagating errors from trees to plots to pixels. *Remote Sensing*
742 *of Environment* 160, 134–143. <https://doi.org/10.1016/j.rse.2015.01.009>.

743 Christensen, W.F., 2011. Filtered kriging for spatial data with heterogeneous measurement error
744 variances. *Biometrics* 67, 947–957. <https://doi.org/10.1111/j.1541-0420.2011.01563.x>.

745 Csillik, O., Asner, G.P., 2020. Near-real time aboveground carbon emissions in peru. *PLOS ONE*
746 15, e0241418. <https://doi.org/10.1371/journal.pone.0241418>.

747 Dieck, R.H., 2007. Measurement uncertainty: methods and applications. ISA.

- 748 Dubayah, R., Blair, J.B., Goetz, S., Fatoyinbo, L., Hansen, M., Healey, S., Hofton, M., Hurtt, G.,
749 Kellner, J., Luthcke, S., Armston, J., Tang, H., Duncanson, L., Hancock, S., Jantz, P., Marselis,
750 S., Patterson, P.L., Qi, W., Silva, C., 2020. The global ecosystem dynamics investigation: High-
751 resolution laser ranging of the earth's forests and topography. *Science of Remote Sensing* 1,
752 100002. <https://doi.org/10.1016/j.srs.2020.100002>.
- 753 Duncanson, L., Armston, J., Disney, M., Avitabile, V., Barbier, N., Calders, K., Carter, S., Chave,
754 J., Herold, M., Crowther, T.W., Falkowski, M., Kellner, J.R., Labrière, N., Lucas, R., MacBean,
755 N., McRoberts, R.E., Meyer, V., Næsset, E., Nickeson, J.E., Paul, K.I., Phillips, O.L., Réjou-
756 Méchain, M., Román, M., Roxburgh, S., Saatchi, S., Schepaschenko, D., Scipal, K., Siqueira,
757 P.R., Whitehurst, A., Williams, M., 2021. Global aboveground biomass product validation best
758 practice protocol <https://doi.org/doi:10.5067>.
- 759 Fazakas, Z., Nilsson, M., Olsson, H., 1999. Regional forest biomass and wood volume estimation
760 using satellite data and ancillary data. *Agricultural and Forest Meteorology* 98-99, 417–425.
761 [https://doi.org/10.1016/s0168-1923\(99\)00112-4](https://doi.org/10.1016/s0168-1923(99)00112-4).
- 762 Feldpausch, T.R., Lloyd, J., Lewis, S.L., Brienen, R.J.W., Gloor, M., Mendoza, A.M., Lopez-
763 Gonzalez, G., Banin, L., Salim, K.A., Affum-Baffoe, K., Alexiades, M., Almeida, S., Amaral,
764 I., Andrade, A., Aragão, L.E.O.C., Murakami, A.A., Arets, E.J.M.M., Arroyo, L., C., G.A.A.,
765 Baker, T.R., Bánki, O.S., Berry, N.J., Cardozo, N., Chave, J., Comiskey, J.A., Alvarez, E.,
766 de Oliveira, A., Fiore, A.D., Djangbletey, G., Domingues, T.F., Erwin, T.L., Fearnside, P.M.,
767 França, M.B., Freitas, M.A., Higuchi, N., Iida, Y., Jiménez, E., Kassim, A.R., Killeen, T.J.,
768 Laurance, W.F., Lovett, J.C., Malhi, Y., Marimon, B.S., Marimon-Junior, B.H., Lenza, E.,
769 Marshall, A.R., Mendoza, C., Metcalfe, D.J., Mitchard, E.T.A., Neill, D.A., Nelson, B.W.,
770 Nilus, R., Nogueira, E.M., Parada, A., Peh, K.S.H., Cruz, A.P., Peñuela, M.C., Pitman, N.C.A.,
771 Prieto, A., Quesada, C.A., Ramírez, F., Ramírez-Angulo, H., Reitsma, J.M., Rudas, A., Saiz,
772 G., Salomão, R.P., Schwarz, M., Silva, N., Silva-Espejo, J.E., Silveira, M., Sonké, B., Stropp, J.,
773 Taedoung, H.E., Tan, S., ter Steege, H., Terborgh, J., Torello-Raventos, M., van der Heijden,
774 G.M.F., Vásquez, R., Vilanova, E., Vos, V.A., White, L., Willcock, S., Woell, H., and, O.L.P.,
775 2012. Tree height integrated into pantropical forest biomass estimates. *Biogeosciences* 9, 3381–
776 3403. <https://doi.org/10.5194/bg-9-3381-2012>.
- 777 GCOS, 2016. The global observing system for climate: Implementation needs, gcos-200.

778 GTOPO30-global, U., 2002. 30-arc second elevation data. US geological survey. National Mapping
779 Division, EROS Data Center. Available from: <http://edcdaac.usgs.gov/gtopo30/gtopo30.html> .

780 Guitet, S., Hérault, B., Molto, Q., Brunaux, O., Couteron, P., 2015. Spatial struc-
781 ture of above-ground biomass limits accuracy of carbon mapping in rainforest but
782 large scale forest inventories can help to overcome. PLOS ONE 10, e0138456.
783 <https://doi.org/10.1371/journal.pone.0138456>.

784 Hansen, M.C., Potapov, P.V., Moore, R., Hancher, M., Turubanova, S.A., Tyukavina, A., Thau,
785 D., Stehman, S.V., Goetz, S.J., Loveland, T.R., Kommareddy, A., Egorov, A., Chini, L., Justice,
786 C.O., Townshend, J.R.G., 2013. High-resolution global maps of 21st-century forest cover change.
787 Science 342, 850–853. <https://doi.org/10.1126/science.1244693>.

788 Harmon, M.E., Fasth, B., Halpern, C.B., Lutz, J.A., 2015. Uncertainty analysis: an evaluation
789 metric for synthesis science. Ecosphere 6, 1–12. <https://doi.org/10.1890/es14-00235.1>.

790 Hernández-Stefanoni, J.L., Castillo-Santiago, M.Á., Mas, J.F., Wheeler, C.E., Andres-Mauricio,
791 J., Tun-Dzul, F., George-Chacón, S.P., Reyes-Palomeque, G., Castellanos-Basto, B., Vaca, R.,
792 Dupuy, J.M., 2020. Improving aboveground biomass maps of tropical dry forests by integrat-
793 ing LiDAR, ALOS PALSAR, climate and field data. Carbon Balance and Management 15.
794 <https://doi.org/10.1186/s13021-020-00151-6>.

795 Herold, M., Carter, S., Avitabile, V., Espejo, A.B., Jonckheere, I., Lucas, R., McRoberts, R.E.,
796 Næsset, E., Nightingale, J., Petersen, R., Reiche, J., Romijn, E., Rosenqvist, A., Rozendaal,
797 D.M.A., Seifert, F.M., Sanz, M.J., Sy, V.D., 2019. The role and need for space-based forest
798 biomass-related measurements in environmental management and policy. Surveys in Geophysics
799 40, 757–778. <https://doi.org/10.1007/s10712-019-09510-6>.

800 Iremonger, S., Gerrand, A., 2011. Global ecological zones for fao forest reporting, 2010. Unpub-
801 lished report. Rome, FAO .

802 Jarvis, A., Reuter, H.I., Nelson, A., Guevara, E., et al., 2008. Hole-filled srtm for the globe version
803 4. available from the CGIAR-CSI SRTM 90m Database (<http://srtm.csi.cgiar.org>) 15, 25–54.

804 Kellogg, K., Hoffman, P., Standley, S., Shaffer, S., Rosen, P., Edelstein, W., Dunn, C.,
805 Baker, C., Barela, P., Shen, Y., Guerrero, A.M., Xaypraseuth, P., Sagi, V.R., Sreekan-
806 tha, C.V., Harinath, N., Kumar, R., Bhan, R., Sarma, C.V.H.S., 2020. NASA-ISRO

807 synthetic aperture radar (NISAR) mission, in: 2020 IEEE Aerospace Conference, IEEE.
808 <https://doi.org/10.1109/aero47225.2020.9172638>.

809 Kyriakidis, P.C., 2004. A geostatistical framework for area-to-point spatial interpolation. *Geo-*
810 *graphical Analysis* 36, 259–289. <https://doi.org/10.1111/j.1538-4632.2004.tb01135.x>.

811 Labriere, N., Tao, S., Chave, J., Scipal, K., Toan, T.L., Abernethy, K., Alonso, A., Barbier, N.,
812 Bissiengou, P., Casal, T., Davies, S.J., Ferraz, A., Herault, B., Jaouen, G., Jeffery, K.J., Kenfack,
813 D., Korte, L., Lewis, S.L., Malhi, Y., Memiaghe, H.R., Poulsen, J.R., Rejou-Mechain, M., Villard,
814 L., Vincent, G., White, L.J.T., Saatchi, S., 2018. *italicin situ/italic* reference datasets from the
815 TropiSAR and AfriSAR campaigns in support of upcoming spaceborne biomass missions. *IEEE*
816 *Journal of Selected Topics in Applied Earth Observations and Remote Sensing* 11, 3617–3627.
817 <https://doi.org/10.1109/jstars.2018.2851606>.

818 Langner, A., Achard, F., Grassi, G., 2014. Can recent pan-tropical biomass maps be used to
819 derive alternative tier 1 values for reporting REDD activities under UNFCCC? *Environmental*
820 *Research Letters* 9, 124008. <https://doi.org/10.1088/1748-9326/9/12/124008>.

821 Liang, J., Crowther, T.W., Picard, N., Wisser, S., Zhou, M., Alberti, G., Schulze, E.D., McGuire,
822 A.D., Bozzato, F., Pretzsch, H., de Miguel, S., Paquette, A., Hérault, B., Scherer-Lorenzen, M.,
823 Barrett, C.B., Glick, H.B., Hengeveld, G.M., Nabuurs, G.J., Pfautsch, S., Viana, H., Vibrans,
824 A.C., Ammer, C., Schall, P., Verbyla, D., Tchebakova, N., Fischer, M., Watson, J.V., Chen,
825 H.Y.H., Lei, X., Schelhaas, M.J., Lu, H., Gianelle, D., Parfenova, E.I., Salas, C., Lee, E.,
826 Lee, B., Kim, H.S., Bruelheide, H., Coomes, D.A., Piotto, D., Sunderland, T., Schmid, B.,
827 Gourlet-Fleury, S., Sonké, B., Tavani, R., Zhu, J., Brandl, S., Vayreda, J., Kitahara, F., Searle,
828 E.B., Neldner, V.J., Ngugi, M.R., Baraloto, C., Frizzera, L., Bałazy, R., Oleksyn, J., Zawila-
829 Niedźwiecki, T., Bouriaud, O., Bussotti, F., Finér, L., Jaroszewicz, B., Jucker, T., Valladares, F.,
830 Jagodzinski, A.M., Peri, P.L., Gonmadje, C., Marthy, W., O'Brien, T., Martin, E.H., Marshall,
831 A.R., Rovero, F., Bitariho, R., Niklaus, P.A., Alvarez-Loayza, P., Chamuya, N., Valencia, R.,
832 Mortier, F., Wortel, V., Engone-Obiang, N.L., Ferreira, L.V., Odeke, D.E., Vasquez, R.M.,
833 Lewis, S.L., Reich, P.B., 2016. Positive biodiversity-productivity relationship predominant in
834 global forests 354. <https://doi.org/10.1126/science.aaf8957>, 10.1126/science.aaf8957.

835 Mahanta, D.J., Borah, M., 2014. Parameter estimation of weibull growth models in forestry.
836 *parameters* 1, 5.

837 Mascaro, J., Asner, G.P., Knapp, D.E., Kennedy-Bowdoin, T., Martin, R.E., Ander-
838 son, C., Higgins, M., Chadwick, K.D., 2014. A tale of two “forests”: Random
839 forest machine learning aids tropical forest carbon mapping. *PLoS ONE* 9, e85993.
840 <https://doi.org/10.1371/journal.pone.0085993>.

841 McRoberts, R.E., Chen, Q., Domke, G.M., Ståhl, G., Saarela, S., Westfall, J.A., 2016. Hybrid
842 estimators for mean aboveground carbon per unit area. *Forest Ecology and Management* 378,
843 44–56. <https://doi.org/10.1016/j.foreco.2016.07.007>.

844 McRoberts, R.E., Næsset, E., Gobakken, T., 2015. The effects of temporal differences between
845 map and ground data on map-assisted estimates of forest area and biomass. *Annals of Forest*
846 *Science* 73, 839–847. <https://doi.org/10.1007/s13595-015-0485-6>.

847 McRoberts, R.E., Næsset, E., Liknes, G.C., Chen, Q., Walters, B.F., Saatchi, S., Herold, M., 2019a.
848 Using a finer resolution biomass map to assess the accuracy of a regional, map-based estimate
849 of forest biomass. *Surveys in Geophysics* 40, 1001–1015. [https://doi.org/10.1007/s10712-019-](https://doi.org/10.1007/s10712-019-09507-1)
850 [09507-1](https://doi.org/10.1007/s10712-019-09507-1).

851 McRoberts, R.E., Næsset, E., Saatchi, S., Liknes, G.C., Walters, B.F., Chen, Q., 2019b. Local
852 validation of global biomass maps. *International Journal of Applied Earth Observation and*
853 *Geoinformation* 83, 101931. <https://doi.org/10.1016/j.jag.2019.101931>.

854 McRoberts, R.E., Næsset, E., Sannier, C., Stehman, S.V., Tomppo, E.O., 2020. Remote sensing
855 support for the gain-loss approach for greenhouse gas inventories. *Remote Sensing* 12, 1891.
856 <https://doi.org/10.3390/rs12111891>.

857 McRoberts, R.E., Tomppo, E.O., 2007. Remote sensing support for national forest inventories. *Re-*
858 *mote Sensing of Environment* 110, 412–419. <https://doi.org/10.1016/j.rse.2006.09.034>.

859 Menlove, J., Healey, S.P., 2020. A comprehensive forest biomass dataset for the USA al-
860 lows customized validation of remotely sensed biomass estimates. *Remote Sensing* 12, 4141.
861 <https://doi.org/10.3390/rs12244141>.

862 Meyer, H., Reudenbach, C., Wöllauer, S., Nauss, T., 2019. Importance of spatial predictor variable
863 selection in machine learning applications – moving from data reproduction to spatial prediction.
864 *Ecological Modelling* 411, 108815. <https://doi.org/10.1016/j.ecolmodel.2019.108815>.

865 Mitchard, E.T., Saatchi, S.S., Baccini, A., Asner, G.P., Goetz, S.J., Harris, N.L., Brown, S., 2013.
866 Uncertainty in the spatial distribution of tropical forest biomass: a comparison of pan-tropical
867 maps. *Carbon Balance and Management* 8. <https://doi.org/10.1186/1750-0680-8-10>.

868 Næsset, E., Bollandsås, O.M., Gobakken, T., Solberg, S., McRoberts, R.E., 2015. The effects of
869 field plot size on model-assisted estimation of aboveground biomass change using multitemporal
870 interferometric SAR and airborne laser scanning data. *Remote Sensing of Environment* 168,
871 252–264. <https://doi.org/10.1016/j.rse.2015.07.002>.

872 Næsset, E., McRoberts, R.E., Pekkarinen, A., Saatchi, S., Santoro, M., Trier, Ø.D., Za-
873 habu, E., Gobakken, T., 2020. Use of local and global maps of forest canopy height
874 and aboveground biomass to enhance local estimates of biomass in miombo woodlands
875 in tanzania. *International Journal of Applied Earth Observation and Geoinformation* ,
876 102138<https://doi.org/10.1016/j.jag.2020.102138>.

877 Nascimento, H.E., Laurance, W.F., 2002. Total aboveground biomass in central amazo-
878 nian rainforests: a landscape-scale study. *Forest Ecology and Management* 168, 311–321.
879 [https://doi.org/10.1016/s0378-1127\(01\)00749-6](https://doi.org/10.1016/s0378-1127(01)00749-6).

880 Nesha, M.K., Herold, M., Sy, V.D., Duchelle, A.E., Martius, C., Branthomme, A., Garzuglia, M.,
881 Jonsson, O., Pekkarinen, A., 2021. An assessment of data sources, data quality and changes
882 in national forest monitoring capacities in the global forest resources assessment 2005-2020.
883 *Environmental Research Letters* <https://doi.org/10.1088/1748-9326/abd81b>.

884 Ploton, P., Mortier, F., Barbier, N., Cornu, G., Réjou-Méchain, M., Rossi, V., Alonso, A.,
885 Bastin, J.F., Bayol, N., Bénédet, F., Bissiengou, P., Chuyong, G., Demarquez, B., Doucet,
886 J.L., Droissart, V., Kamdem, N.G., Kenfack, D., Memiaghe, H., Moses, L., Sonké, B., Texier,
887 N., Thomas, D., Zebaze, D., Péliissier, R., Gourlet-Fleury, S., 2020a. A map of african humid
888 tropical forest aboveground biomass derived from management inventories. *Scientific Data* 7.
889 <https://doi.org/10.1038/s41597-020-0561-0>.

890 Ploton, P., Mortier, F., Réjou-Méchain, M., Barbier, N., Picard, N., Rossi, V., Dormann, C.,
891 Cornu, G., Viennois, G., Bayol, N., Lyapustin, A., Gourlet-Fleury, S., Péliissier, R., 2020b.
892 Spatial validation reveals poor predictive performance of large-scale ecological mapping models.
893 *Nature Communications* 11. <https://doi.org/10.1038/s41467-020-18321-y>.

- 894 Quegan, S., Ciais, P., 2018. User Requirement Document. Technical Report. European Space
895 Agency.
- 896 Quegan, S., Toan, T.L., Chave, J., Dall, J., Exbrayat, J.F., Minh, D.H.T., Lomas, M.,
897 D'Alessandro, M.M., Paillou, P., Papathanassiou, K., Rocca, F., Saatchi, S., Scipal, K., Shugart,
898 H., Smallman, T.L., Soja, M.J., Tebaldini, S., Ulander, L., Villard, L., Williams, M., 2019. The
899 european space agency BIOMASS mission: Measuring forest above-ground biomass from space.
900 *Remote Sensing of Environment* 227, 44–60. <https://doi.org/10.1016/j.rse.2019.03.032>.
- 901 Réjou-Méchain, M., Barbier, N., Couteron, P., Ploton, P., Vincent, G., Herold, M., Mermoz, S.,
902 Saatchi, S., Chave, J., de Boissieu, F., Féret, J.B., Takoudjou, S.M., Péliissier, R., 2019. Upscaling
903 forest biomass from field to satellite measurements: Sources of errors and ways to reduce them.
904 *Surveys in Geophysics* 40, 881–911. <https://doi.org/10.1007/s10712-019-09532-0>.
- 905 Réjou-Méchain, M., Muller-Landau, H.C., Detto, M., Thomas, S.C., Toan, T.L., Saatchi, S.S.,
906 Barreto-Silva, J.S., Bourg, N.A., Bunyavejchewin, S., Butt, N., Brockelman, W.Y., Cao, M.,
907 Cárdenas, D., Chiang, J.M., Chuyong, G.B., Clay, K., Condit, R., Dattaraja, H.S., Davies, S.J.,
908 Duque, A., Esufali, S., Ewango, C., Fernando, R.H.S., Fletcher, C.D., Gunatilleke, I.A.U.N., Hao,
909 Z., Harms, K.E., Hart, T.B., Hérault, B., Howe, R.W., Hubbell, S.P., Johnson, D.J., Kenfack, D.,
910 Larson, A.J., Lin, L., Lin, Y., Lutz, J.A., Makana, J.R., Malhi, Y., Marthews, T.R., McEwan,
911 R.W., McMahon, S.M., McShea, W.J., Muscarella, R., Nathalang, A., Noor, N.S.M., Nytch, C.J.,
912 Oliveira, A.A., Phillips, R.P., Pongpattananurak, N., Punchi-Manage, R., Salim, R., Schurman,
913 J., Sukumar, R., Suresh, H.S., Suwanvecho, U., Thomas, D.W., Thompson, J., Uriarte, M.,
914 Valencia, R., Vicentini, A., Wolf, A.T., Yap, S., Yuan, Z., Zartman, C.E., Zimmerman, J.K.,
915 Chave, J., 2014. Local spatial structure of forest biomass and its consequences for remote sensing
916 of carbon stocks. *Biogeosciences* 11, 6827–6840. <https://doi.org/10.5194/bg-11-6827-2014>.
- 917 Réjou-Méchain, M., Tanguy, A., Piponiot, C., Chave, J., Hérault, B., 2017. biomass: an r package
918 for estimating above-ground biomass and its uncertainty in tropical forests. *Methods in Ecology
919 and Evolution* 8, 1163–1167. <https://doi.org/10.1111/2041-210x.12753>.
- 920 Rodríguez-Veiga, P., Quegan, S., Carreiras, J., Persson, H.J., Fransson, J.E., Hoscilo, A.,
921 Ziółkowski, D., Stereńczak, K., Lohberger, S., Stängel, M., Berninger, A., Siegert, F., Avitabile,
922 V., Herold, M., Mermoz, S., Bouvet, A., Toan, T.L., Carvalhais, N., Santoro, M., Cartus, O.,
923 Rauste, Y., Mathieu, R., Asner, G.P., Thiel, C., Pathe, C., Schnullius, C., Seifert, F.M., Tansey,

924 K., Balzter, H., 2019. Forest biomass retrieval approaches from earth observation in different
925 biomes. *International Journal of Applied Earth Observation and Geoinformation* 77, 53–68.
926 <https://doi.org/10.1016/j.jag.2018.12.008>.

927 Rodríguez-Veiga, P., Saatchi, S., Tansey, K., Balzter, H., 2016. Magnitude, spatial distribution and
928 uncertainty of forest biomass stocks in Mexico. *Remote Sensing of Environment* 183, 265–281.
929 <https://doi.org/10.1016/j.rse.2016.06.004>.

930 Rodríguez-Veiga, P., Wheeler, J., Louis, V., Tansey, K., Balzter, H., 2017. Quan-
931 tifying forest biomass carbon stocks from space. *Current Forestry Reports* 3, 1–18.
932 <https://doi.org/10.1007/s40725-017-0052-5>.

933 Saatchi, S., Marlier, M., Chazdon, R.L., Clark, D.B., Russell, A.E., 2011a. Impact of spatial
934 variability of tropical forest structure on radar estimation of aboveground biomass. *Remote*
935 *Sensing of Environment* 115, 2836–2849. <https://doi.org/10.1016/j.rse.2010.07.015>.

936 Saatchi, S.S., Harris, N.L., Brown, S., Lefsky, M., Mitchard, E.T.A., Salas, W., Zutta, B.R.,
937 Buermann, W., Lewis, S.L., Hagen, S., Petrova, S., White, L., Silman, M., Morel, A., 2011b.
938 Benchmark map of forest carbon stocks in tropical regions across three continents. *Proceedings*
939 *of the National Academy of Sciences* 108, 9899–9904. <https://doi.org/10.1073/pnas.1019576108>.

940 Santoro, M., 2020. CCI Biomass Product User Guide v2. Technical Report. European Space
941 Agency.

942 Santoro, M., Beaudoin, A., Beer, C., Cartus, O., Fransson, J.E., Hall, R.J., Pathe, C., Schullius,
943 C., Schepaschenko, D., Shvidenko, A., Thurner, M., Wegmüller, U., 2015. Forest growing stock
944 volume of the northern hemisphere: Spatially explicit estimates for 2010 derived from Envisat
945 ASAR. *Remote Sensing of Environment* 168, 316–334. <https://doi.org/10.1016/j.rse.2015.07.005>.

946 Santoro, M., Beer, C., Cartus, O., Schullius, C., Shvidenko, A., McCallum, I., Wegmüller, U.,
947 Wiesmann, A., 2011. Retrieval of growing stock volume in boreal forest using hyper-temporal
948 series of Envisat ASAR ScanSAR backscatter measurements. *Remote Sensing of Environment*
949 115, 490–507. <https://doi.org/10.1016/j.rse.2010.09.018>.

950 Santoro, M., Cartus, O., 2019. Esa biomass climate change initiative (biomass_cci):
951 Global datasets of forest above-ground biomass for the year 2017, v1.
952 <https://doi.org/10.5285/BEDC59F37C9545C981A839EB552E4084>.

953 Santoro, M., Cartus, O., Carvalhais, N., Rozendaal, D., Avitabile, V., Araza, A., de Bruin, S.,
954 Herold, M., Quegan, S., Veiga, P.R., Balzter, H., Carreiras, J., Schepaschenko, D., Korets,
955 M., Shimada, M., Itoh, T., Martínez, Á.M., Cavlovic, J., Gatti, R.C., da Conceição Bispo, P.,
956 Dewnath, N., Labrière, N., Liang, J., Lindsell, J., Mitchard, E.T.A., Morel, A., Pascagaza,
957 A.M.P., Ryan, C.M., Slik, F., Laurin, G.V., Verbeeck, H., Wijaya, A., Willcock, S., 2020.
958 The global forest above-ground biomass pool for 2010 estimated from high-resolution satellite
959 observations <https://doi.org/10.5194/essd-2020-148>.

960 Schepaschenko, D., Chave, J., Phillips, O.L., Lewis, S.L., Davies, S.J., Réjou-Méchain, M., Sist, P.,
961 Scipal, K., Perger, C., Herault, B., Labrière, N., Hofhansl, F., Affum-Baffoe, K., Aleinikov, A.,
962 Alonso, A., Amani, C., Araujo-Murakami, A., Armston, J., Arroyo, L., Ascarrunz, N., Azevedo,
963 C., Baker, T., Bałazy, R., Bedeau, C., Berry, N., Bilous, A.M., Bilous, S.Y., Bissiengou, P., Blanc,
964 L., Bobkova, K.S., Braslavskaya, T., Brienen, R., Burslem, D.F.R.P., Condit, R., Cuni-Sanchez,
965 A., Danilina, D., del Castillo Torres, D., Derroire, G., Descroix, L., Sotta, E.D., d'Oliveira,
966 M.V.N., Dresel, C., Erwin, T., Evdokimenko, M.D., Falck, J., Feldpausch, T.R., Foli, E.G.,
967 Foster, R., Fritz, S., Garcia-Abril, A.D., Gornov, A., Gornova, M., Gothard-Bassébé, E., Gourlet-
968 Fleury, S., Guedes, M., Hamer, K.C., Susanty, F.H., Higuchi, N., Coronado, E.N.H., Hubau, W.,
969 Hubbell, S., Ilstedt, U., Ivanov, V.V., Kanashiro, M., Karlsson, A., Karminov, V.N., Killeen,
970 T., Koffi, J.C.K., Konovalova, M., Kraxner, F., Krejza, J., Krisnawati, H., Krivobokov, L.V.,
971 Kuznetsov, M.A., Lakyda, I., Lakyda, P.I., Licona, J.C., Lucas, R.M., Lukina, N., Lussetti,
972 D., Malhi, Y., Manzanera, J.A., Marimon, B., Junior, B.H.M., Martinez, R.V., Martynenko,
973 O.V., Matsala, M., Matyashuk, R.K., Mazzei, L., Memiaghe, H., Mendoza, C., Mendoza, A.M.,
974 Moroziuk, O.V., Mukhortova, L., Musa, S., Nazimova, D.I., Okuda, T., Oliveira, L.C., Ontikov,
975 P.V., Osipov, A.F., Pietsch, S., Playfair, M., Poulsen, J., Radchenko, V.G., Rodney, K., Rozak,
976 A.H., Ruschel, A., Rutishauser, E., See, L., Shchepashchenko, M., Shevchenko, N., Shvidenko,
977 A., Silveira, M., Singh, J., Sonké, B., Souza, C., Stereńczak, K., Stonozhenko, L., Sullivan,
978 M.J.P., Szatniewska, J., Taedoung, H., ter Steege, H., Tikhonova, E., Toledo, M., Trefilova,
979 O.V., Valbuena, R., Gamarra, L.V., Vasiliev, S., Vedrova, E.F., Verhovets, S.V., Vidal, E.,
980 Vladimirova, N.A., Vleminckx, J., Vos, V.A., Vozmitel, F.K., Wanek, W., West, T.A.P., Woell,
981 H., Woods, J.T., Wortel, V., Yamada, T., Hajar, Z.S.N., Zo-Bi, I.C., 2019. The forest observation
982 system, building a global reference dataset for remote sensing of forest biomass. *Scientific Data*
983 6. <https://doi.org/10.1038/s41597-019-0196-1>.

984 Schimel, D., Pavlick, R., Fisher, J.B., Asner, G.P., Saatchi, S., Townsend, P., Miller, C., Franken-
985 berg, C., Hibbard, K., Cox, P., 2015. Observing terrestrial ecosystems and the carbon cycle from
986 space. *Global Change Biology* 21, 1762–1776. <https://doi.org/10.1111/gcb.12822>.

987 Suarez, D.R., Rozendaal, D.M.A., Sy, V.D., Phillips, O.L., Alvarez-Dávila, E., Anderson-Teixeira,
988 K., Araujo-Murakami, A., Arroyo, L., Baker, T.R., Bongers, F., Brienen, R.J.W., Carter,
989 S., Cook-Patton, S.C., Feldpausch, T.R., Griscom, B.W., Harris, N., Hérault, B., Coronado,
990 E.N.H., Leavitt, S.M., Lewis, S.L., Marimon, B.S., Mendoza, A.M., N'dja, J.K., N'Guessan,
991 A.E., Poorter, L., Qie, L., Rutishauser, E., Sist, P., Sonké, B., Sullivan, M.J.P., Vilanova, E.,
992 Wang, M.M.H., Martius, C., Herold, M., 2019. Estimating aboveground net biomass change for
993 tropical and subtropical forests: Refinement of IPCC default rates using forest plot data. *Global*
994 *Change Biology* 25, 3609–3624. <https://doi.org/10.1111/gcb.14767>.

995 Toan, T.L., Quegan, S., Davidson, M., Balzter, H., Paillou, P., Papathanassiou, K., Plummer, S.,
996 Rocca, F., Saatchi, S., Shugart, H., Ulander, L., 2011. The BIOMASS mission: Mapping global
997 forest biomass to better understand the terrestrial carbon cycle. *Remote Sensing of Environment*
998 115, 2850–2860. <https://doi.org/10.1016/j.rse.2011.03.020>.

999 Tsutsumida, N., Rodríguez-Veiga, P., Harris, P., Balzter, H., Comber, A., 2019. Investigating
1000 spatial error structures in continuous raster data. *International Journal of Applied Earth Ob-*
1001 *servation and Geoinformation* 74, 259–268. <https://doi.org/10.1016/j.jag.2018.09.020>.

1002 UN-FAO, 2010. *Global Forest Resources Assessment 2010: Main report*. Technical Report.

1003 UN-FAO, 2020. *Global Forest Resources Assessment 2020*. Technical Report.

1004 Wager, S., Hastie, T., Efron, B., 2014. Confidence intervals for random forests: The jackknife and
1005 the infinitesimal jackknife. *The Journal of Machine Learning Research* 15, 1625–1651.

1006 Whittaker, R., 1975. Whittaker biome diagram.

1007 Wright, M.N., Ziegler, A., 2017. ranger: A fast implementation of random forests for high dimen-
1008 sional data in c and r. *Journal of Statistical Software* 77. <https://doi.org/10.18637/jss.v077.i01>.

1009 Xu, L., Saatchi, S.S., Yang, Y., Yu, Y., Pongratz, J., Bloom, A.A., Bowman, K., Worden, J., Liu,
1010 J., Yin, Y., Domke, G., McRoberts, R.E., Woodall, C., Nabuurs, G.J., de Miguel, S., Keller,
1011 M., Harris, N., Maxwell, S., Schimel, D., 2021. Changes in global terrestrial live biomass over

1012 the 21st century. *Science Advances* 7, eabe9829. <https://doi.org/10.1126/sciadv.abe9829>,
1013 10.1126/sciadv.abe9829.

1014 Xu, L., Saatchi, S.S., Yang, Y., Yu, Y., White, L., 2016. Performance of non-parametric algo-
1015 rithms for spatial mapping of tropical forest structure. *Carbon Balance and Management* 11.
1016 <https://doi.org/10.1186/s13021-016-0062-9>.

1017 Zhang, Q., Liang, Y., He, H., 2018. Tree-lists estimation for chinese boreal forests by integrating
1018 weibull diameter distributions with MODIS-based forest attributes from kNN imputation. *Forests*
1019 9, 758. <https://doi.org/10.3390/f9120758>.

1020 Zhang, X., Duan, A., Zhang, J., Xiang, C., 2014. Estimating tree height-diameter models with the
1021 bayesian method. *The Scientific World Journal* 2014, 1–9. <https://doi.org/10.1155/2014/683691>.

1022 Zhang, Y., Liang, S., 2020. Fusion of multiple gridded biomass datasets for generating a global
1023 forest aboveground biomass map. *Remote Sensing* 12, 2559. <https://doi.org/10.3390/rs12162559>.

1024 Zhang, Y., Liang, S., Yang, L., 2019. A review of regional and global gridded forest biomass
1025 datasets. *Remote Sensing* 11, 2744. <https://doi.org/10.3390/rs11232744>.

1026 Zhao, P., Lu, D., Wang, G., Wu, C., Huang, Y., Yu, S., 2016. Examining spectral reflectance
1027 saturation in landsat imagery and corresponding solutions to improve forest aboveground biomass
1028 estimation. *Remote Sensing* 8, 469. <https://doi.org/10.3390/rs8060469>.